A Scientific Investigation into Concrete Pavement Durability

January 2021

Massachusetts Institute of Technology
R. Pellenq*, M. Bazant, T. Divoux*, A. Dufresne*, R. Dupuis*, J. Gregory,
K. Ioannidou*, S. Yip, T. Zhou*, F. Ulm

Oregon State University
J. Weiss, R. Ghantous, J. Ideker, C. Qiao, P. Suraneni*

University of New Brunswick
M. Thomas, T. Moffatt*

Additional Contributors
J. Areyro (U. of Kuwait), M. Haist (U. of Hannover), F. Rajabipour (Penn. State),
J. Rose (CEREGE, CNRS/Aix-Marseille U.), L. Beland (Queen's U.)

Industry Advisory Board
L. Barcelo* (LafargeHolcim), M. Ben Haha (Heidelberg), C. Lobo (NRMCA), N. Popoff (Votorantim),
P. Tennis (PCA), S. Tritsch (CP Tech Center)

*Former affiliation

This research was jointly funded by the Portland Cement Association and the Ready Mixed Concrete Research and Education Foundation

Executive Summary

Although concrete pavements offer many long-term performance benefits, there are still instances where premature degradation of pavements leads to unexpected and costly repairs. In addition to being a burden to transportation agencies and the driving public, these situations have the potential to unduly tarnish the reputation of concrete pavements.

We assembled a multidisciplinary team across multiple universities whose objective was to improve the durability of concrete pavements by improving the scientific understanding of pavement distresses. In particular, we sought to develop a quantitative understanding of the chemical reactions to the physical manifestation of concrete pavement damage from alkali–silica reaction (ASR) and freeze-thaw (FT). This will lay the foundation for connecting pavement material properties and fracture and durability prediction, while also helping to establish the potential for ASR and/or FT damage in a concrete pavement and the rate at which it would happen. In essence, it will identify the conditions that lead to ASR or FT damage.

The research approach involved a range of experiments including nano-scale chemomechanical characterization of ASR gels, mechanical and thermal characterization of cement paste after meso-scale FT cycling, and likelihood of ASR damage for concrete mixtures. The modeling approach included analytical and simulation models of ASR, FT, and fracture at the nano-, meso-, and micro scales.

The key outcome of this project is a unified theoretical framework for explaining both ASR and FT damage. Detailed explanations for both mechanisms are as follows.

FT: by combining mechanical and characterization experiments together with atomistic and mesoscale simulations, we found that there is NO direct impact of an ice phase in damage to the paste and concrete. FT damage in concrete/cement paste appears to result from a disjoining ionic pressure at the C-S-H/ice interface in the capillary pore network which is that fractures the C-S-H matrix. Computer-simulated effects with the type and concentration of ions in the pore solution agree well with experiments.

ASR: by combining mechanical and characterization experiments together with atomistic and mesoscale simulations, we found that the swelling of ASR gel is NOT the reason for damage to concrete. ASR damage is likely the consequence of a Na^{+} ⟷ Ca^{2+} exchange mechanism between an initially formed alkali gel that is deficient in Ca (Ca-poor) and C-S-H. Over time this exchange creates a disjoining ionic pressure at the interface between C-S-H and calcified ASR gel (Ca-rich) in the capillary pore network that causes expansion and cracking within the C-S-H matrix.

1 Motivation: Some concrete pavements are not reaching their full lifetime potential due to durability issues

Although concrete pavements offer many long-term performance benefits, there are still instances where premature degradation of pavements leads to unexpected and costly repairs. In addition to being a burden to transportation agencies and the drivers in those states, these situations have the potential to unduly tarnish the reputation of concrete pavements. Therefore, further improving concrete pavement durability is a critical component of improving perceived reliability, reducing maintenance costs for DOTs, and reducing fuel costs for drivers. Peter Taylor at the National Concrete Pavement Technology Center defines concrete durability as "the ability of the concrete to survive the environment to which it is exposed." [1] Two of the important failure mechanisms in concrete pavements that Taylor notes as affecting durability are internal attack by alkali–silica (alkali-aggregate) reaction (ASR) and cold weather freeze-thaw (FT) cycling. Although these mechanisms have been studied for many years and a thorough *qualitative* understanding of them exists, current durability models based on experimental methods do not adequately predict pavement degradation by these mechanisms. This is primarily due to the fact that there has been minimal work in developing *quantitative* models of ASR and FT induced degradation. In addition, pavement durability models do not directly account for material properties. So if a new type of pavement material is used, the durability performance of the material cannot be quantified without extensive testing.

References

1. P. Taylor, "Long-Life Concrete: How Long Will My Concrete Last?", National Concrete Pavement Technology Center, 2013, http://www.cptechcenter.org/technical-library/documents/durability_synthesis_w_cvr.pdf.

2 Approach: A new way of improving the durability of concrete pavements

We assembled a team whose objective was to improve the durability of concrete pavements by improving the scientific understanding of pavement distresses and translating this into engineering practice. Our primary goal for the project was to develop a quantitative understanding of the chemical reactions to the physical manifestation of concrete pavement damage from ASR and freeze-thaw. This informs pavement design. The outcomes of this work could then inform efforts to quantify the economic and environmental benefits of durable concrete pavements (relative to those that prematurely fail). This informs material selection.

Our vision is that the research will connect pavement material properties and durability performance prediction. It will also help to establish the potential for ASR/FT damage in a concrete pavement and the rate at which it would happen. In essence, it will identify the conditions that lead to ASR/FT damage.

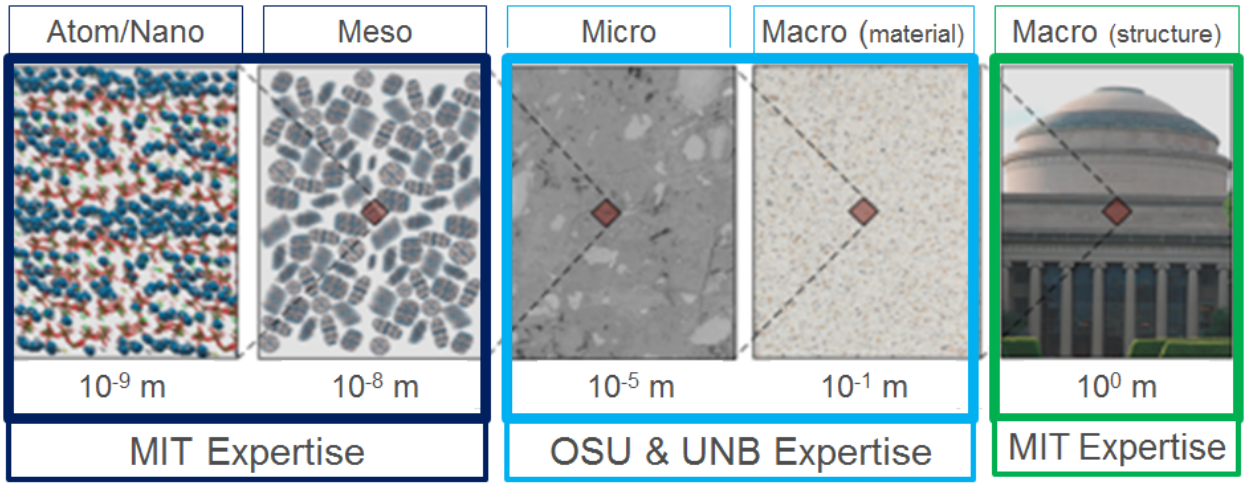

Figure 1 – The scales that will be analyzed in the project and the expertise of the project partners.

A multiscale approach is required to connect the scientific degradation mechanisms that occur at very small scales with the technical, economic, and environmental analyses at large scales, see Figure 1. Our multidisciplinary team consisted of researchers primarily from three universities: the Massachusetts Institute of Technology (MIT), Oregon State University (OSU), and the University of New Brunswick (UNB). (Collaborators also participated from a few other universities.) The researchers have expertise in experimental and modeling methods at a range of scales and on a variety of topics including materials science, civil engineering, economics, and life cycle assessment (the method for quantifying life cycle environmental impacts). The scientific approach for the project is outlined in Figure 2. It involved chemomechanical (both chemistry and mechanics) characterization of mechanisms. Damage is the manifestation of the distress mechanism in the pavement, and this is caused by the mechanics of expansion within the concrete, either due to ASR gel or FT cycling of water. The expansion is due to a combination of chemistry and kinetics that enable the creation of ASR gel or ionic pore solution. Research activities in the project included conducting experiments to improve our understanding of the mechanisms taking place at small scales, models to quantify these

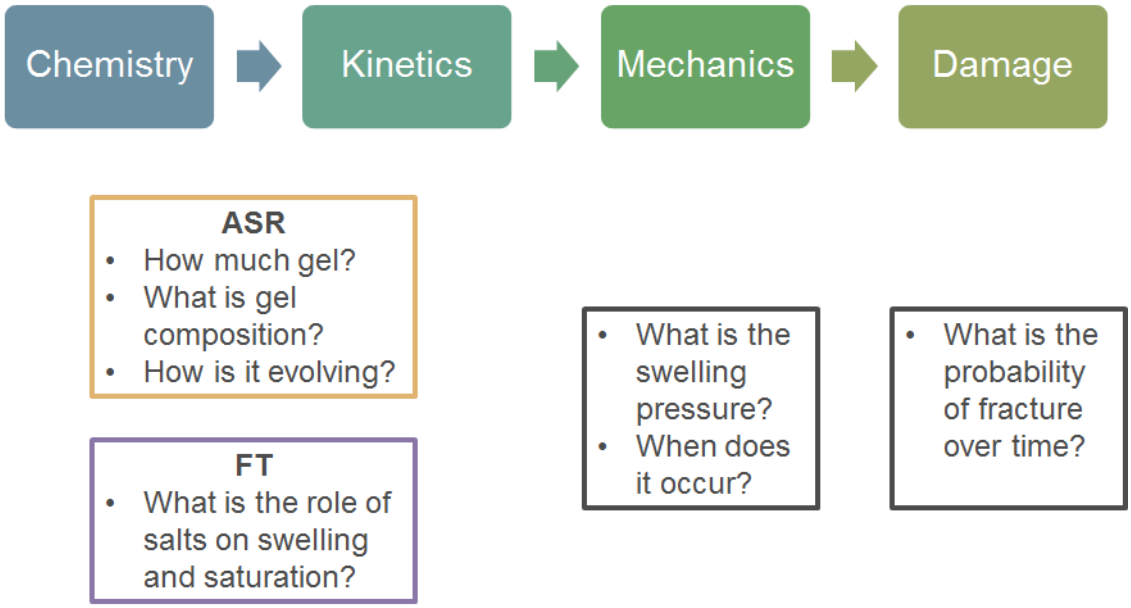

Figure 2 – Scientific approach for the project: chemomechanical characterization of mechanisms.

mechanisms, and calibration and validation experiments on concrete specimens. Specific activities for researchers from the three institutions are summarized in Figure 3. The figure demonstrates the collaborative nature of the project and the interconnected nature of the research activities. MIT conducted experimental and modeling efforts at the small scale, while OSU and UNB provided experimental data that acts as inputs to MIT models, as well as validation of MIT models. In addition, they developed performance tests that will improve evaluations of paving materials for potential degradation.

MIT Concrete Sustainability Hub (CSHub) researchers, led by Prof. Franz Ulm and Dr. Roland Pellenq, conducted the following activities:

- Nano and meso-scale chemomechanical characterization experiments of ASR gels and FT mechanisms using techniques such as nanoindentation, x-ray diffraction, and tomography.
- Development of nano and meso-scale models of ASR and FT using molecular dynamics and analytical simulation models.

OSU researchers, led by Prof. Jason Weiss, conducted the following activities around the characterization of FT cycling and deicer interactions:

- Experimental characterization of desorption isotherms, rate of saturation due to diffuse damage, and stresses induced in concrete due to FT cycling.
- Modeling of damage gradients from FT cycling.
- Creation of a new performance-based design specification for durability.
- Calibration and validation of CSHub FT models.

UNB researchers, led by Prof. Michael Thomas, conducted the following activities around the experimental characterization of ASR:

- Development of a database linking conditions and ASR effects dependent on cement chemistry, aggregate mineralogy, temperature, and moisture availability.
- Creation of a new ASR performance test.
- Calibration and validation of CSHub ASR models.

The results of this research effort are detailed in chapters on ASR (3) and FT (4). Finally, the outlook for future research is detailed in Chapter 5.

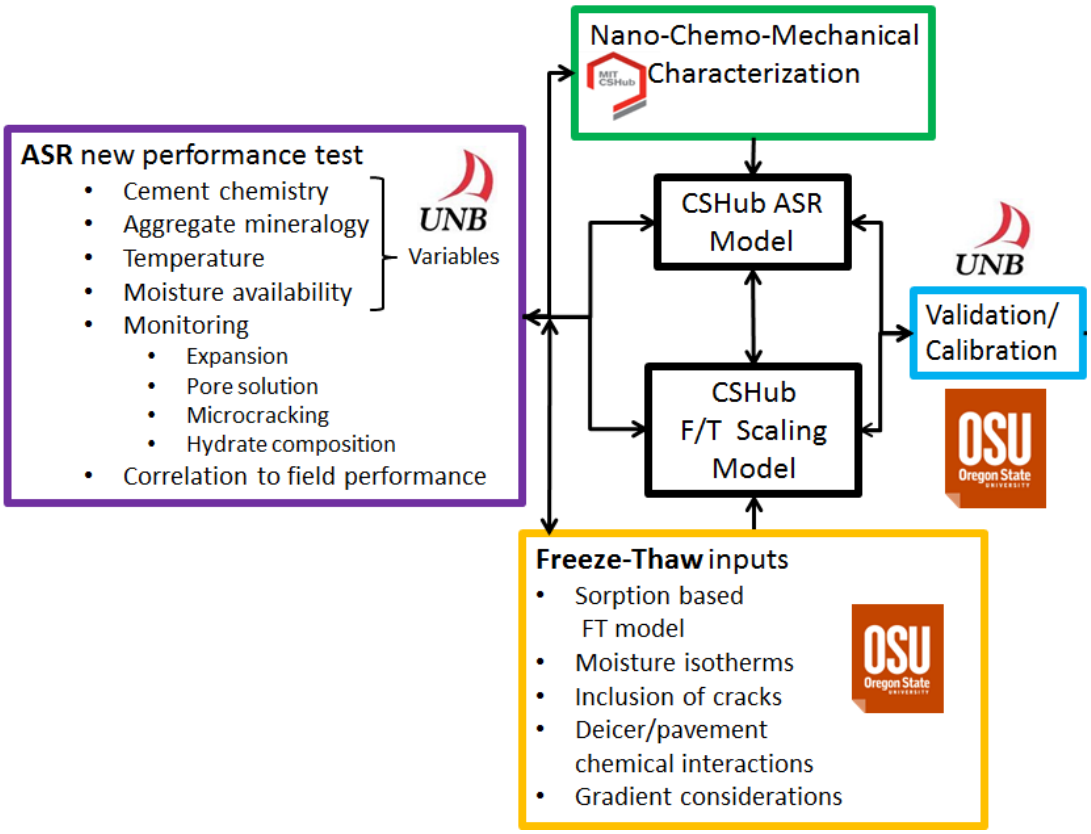

Figure 3 – Research activities for the three research partners: the MIT Concrete Sustainability Hub (CSHub), Oregon State University (OSU), and the University of New Brunswick (UNB).

3 Alkali-silica reaction: what causes the expansive pressure in ASR-affected concrete?

Although extensive research has been conducted to study the conditions that lead to ASR and approaches to mitigate or avoid its effects, there remains gaps in the understanding of the mechanisms that lead ASR to induce damage in concrete. There are two main theories about the cause of the pressure that leads to damage:

A. The ASR gel directly creates the pressure.

B. The ASR gel indirectly creates the pressure.

To a large extent, the mechanisms by which the ASR gel is formed does not vary much from one theory to another. It requires a high-pH solution and the presence of alkali (Na and K) ions.
Examples of mechanisms for theory A (ASR gel directly creates pressure) are as follows:

A1. Dunant and Scrivener [5] suggest that the ASR gel is a very hard material (~0.5 hardness of C-S-H) that can exert considerable pressure on C-S-H since it generates 10-20% more solids volume of the reaction products (gel) than the aggregate that it dissolves.

A2. Ichikawa and Miura [6] suggest that the gel initially has a low-calcium content and flows out without creating damage. It calcifies in the cement paste. It is suggested that this calcified gel layer is semi-permeable: it lets alkali ions, OH- and water flow, but does not let gel escape. The ASR reaction continues, with the additional gel produced confined by the calcified reaction rim. This leads to a buildup of expansive pressure.

A3. Multon et al [9], Liaudat et al [7], Alnaggar et al [1,2], Charpin [4] consider that the gel is a largely incompressible fluid that can flow in the inter-facial transition zone (ITZ) between the aggregates and cement paste, but that cannot flow in cement paste.

A4. Bazant & Rahimi-Aghdam [3] suggest that the gel is a viscous fluid that is described by a Darcy flow. They suggest that it calcifies when it flows in the cement paste—where it shrinks and no longer generates expansive pressure. Through a high rate of ions and water intake in the aggregate and a high gel viscosity—or, equivalently, low permeability of the material to the gel—a high pressure is necessary to permit flow of the gel.

Evidence refuting these mechanisms is as follows:

A1. This model depends on ASR gel having an indentation modulus of 10-30 GPa. These values are observed by Leeman and Lura [8]. However, these ASR samples were dried before measurements. Similar measurements by Divoux (MIT/CNRS) (Section 3.1.1) shows that the indentation modulus of ASR gels is negligible at 80-90% relative humidity.

A2. There is no evidence as to the flow properties of water, ions, and gel through cement paste filled with calcified ASR gel.

A3. and A4. There is little evidence as to the rheology of ASR-gels. One experiment has been reported by Vayghan, Rajabipour, and Rosenberger [10]. They measured the yield stress of a lab-synthesized gel. They obtain values of the order of 10 kPa. In a seminal experimental work, Struble and Diamond [18] studied the swelling properties of synthetic alkali-silica gels and showed that no correlation exists between amount of swelling and swelling pressure. However, large swelling pressure (up to 11 MPa) could be achieved at a very specific range of sodium concentrations (Na_2O:SiO_2 mole ratio = 0.34). In this work, no correlation was found between the water content of the alkali-silica gels and the swelling pressure. Globally, the implications of Struble and Diamond's findings with respect to the alkali-silica reaction problem in concrete are that one should NOT assume that gels produced by such reactions necessarily is capable of exerting a deleterious effect on the concrete. Many such gels are undoubtedly insufficiently capable of swelling or exerting sufficient swelling pressure to crack the concrete, and so may not provide external evidence of their existence by appearance or by effect.

Examples of mechanisms for theory B (ASR gel indirectly creates pressure) are as follows:

B1. As the gel flows into the cement paste, it exchanges ions with the nearby cement paste. Notably, the C-S-H intakes alkali ions (and loses calcium), which leads to expansion of the C-S-H grains. This is referred to as alkali-induced C-S-H swelling. In this model, the ASR gel concentrates the alkali as it is formed, and releases as it exchanges alkali ions for calcium, exposing the C-S-H to high local alkali concentrations, relative to the average alkali content of the cement paste. These transients may leads to deterioration of the C-S-H.

B2. The gel flows into the cement paste. It fills up meso- and nano-pores. However, a nano-scale wetting layer remains between the C-S-H and the gel, providing a pathway for ion diffusion. As ions accumulate in this wetting nanolayer, an ionic disjoining pressure develops between the charged C-S-H surface and the neutral (or nearly neutral) ASR gel surface. However, the initially sodium- and water-rich gel has very little mechanical properties as experimentally shown by Divoux (CNRS/MIT) using nano-indentation (Section 3.1.1). Therefore, alkali-rich and hydrated ASR gels cannot sustain large disjoining ionic pressures, and the ASR gels flow into nearby pores. Since pressure cannot buildup, no ASR damage develops. Over time (on the order of 10 years), there is sodium-to-calcium replacement taking place in the ASR gel that rigidifies the gel (calcium is more of a glass former than sodium). The Na concentration in the wetting layer between the ASR gel and the C-S-H increases, which has the primary effect of increasing the ionic disjoining pressure. These two concomitant effects (ASR gel rigidifying and increase of the ionic disjoining pressure in the wetting layer at the C-S-H pore surface) now create the conditions of indirect damage to the cement paste as the rigid calcium-rich ASR gel vein can sustain the ionic disjoining pressure that is then transmitted to the C-S-H matrix, creating damage (see Figure 4). The intake of sodium in C-S-H induces limited C-S-H swelling, (B1). This scenario also allows for alkali recycling, as the ASR gel returns its Na and K to the pore solution.

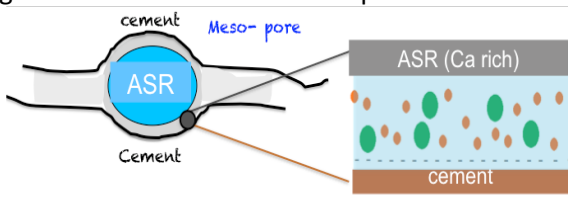

Figure 4: illustration of the osmotic pressure in the interfacial nanometers-thick electrolyte layer between C-S-H and a Ca-loaded ASR gel.

3.1 Experimental investigation of ASR mechanisms

3.1.1 Experiments on rheology of ASR gels (synthetic gels, synthetic systems, natural systems)

In this first subsection, we report on the mechanical properties of ASR gels encountered in concrete. The form of silica minerals occurring in some types of aggregates is dissolved by reacting with hydroxyl ions in the pore solution, subsequently forming a weak alkali-silica gel. Alternatively, the dissolved silica can cross-link (e.g., in presence of calcium ions), coagulate, and form a more rigid ASR gel [12]. To date, the mechanical properties of ASR gels have been studied in configurations that strongly differ from the native state of the ASR gel. Indeed, ASR gels are either synthesized in the lab [13] or, when extracted from natural samples, ASR gels are systematically dried prior to any mechanical testing. Experiments on the latter type of desiccated gels leads to the erroneous conclusion that ASR gels display strong mechanical properties comparable to that of hard solids, with a Young's modulus of the order of $10\ GPa$ [14,15] and a fracture toughness of about $0.6\ MPa$ [15]. The goal of our experiments was to probe the mechanical properties of pristine ASR gels formed naturally in concrete samples. The ultimate goal was to infer from such testing the in situ mechanical properties of ASR gels, in the limit of saturated moisture content.

The first key result comes from nano-indentation experiments on a pristine ASR gel. Mortar samples, which were prepared with reactive aggregates by the team at University of New Brunswick (UNB), were incubated at MIT in saturated humidity conditions for about a year to favor the development of ASR gel pockets. Samples were cut open and examined by stereomicroscopy to locate regions of ASR gels (Figure 5, top). While performing such observations, we immediately noticed that the gel samples, being exposed to atmospheric humidity, were drying over the course of hours. In order to quantify the effect of drying on the properties of ASR gel, we performed the following experiment: we identified a region of ASR gel of remarkable large size (~200 µm) that we placed in a testing chamber of controlled relative humidity (ranging between 50% and 60%) for 5 days, during which we performed mechanical testing. Note that the sub-micrometer size of the ASR gel pocket necessitates the use of a precise and localized investigation technique to measure the mechanical properties of the gel. We chose to use nano-indentation, which consists in loading the sample using an indenter following a prescribed load profile, whilst measuring the depth of the indenter during such sequence. The test is repeated at different locations and analyzed following the method developed by Oliver & Pharr [16]. Each indentation test is limited to a maximum depth of 300 nm and leads to a local estimate of the sample indentation modulus (M) and hardness (H). The former quantity tells us about the linear elastic property of the gel, whereas the latter quantity measures the resistance of the gel to a localized plastic deformation. At first, right after cutting open the

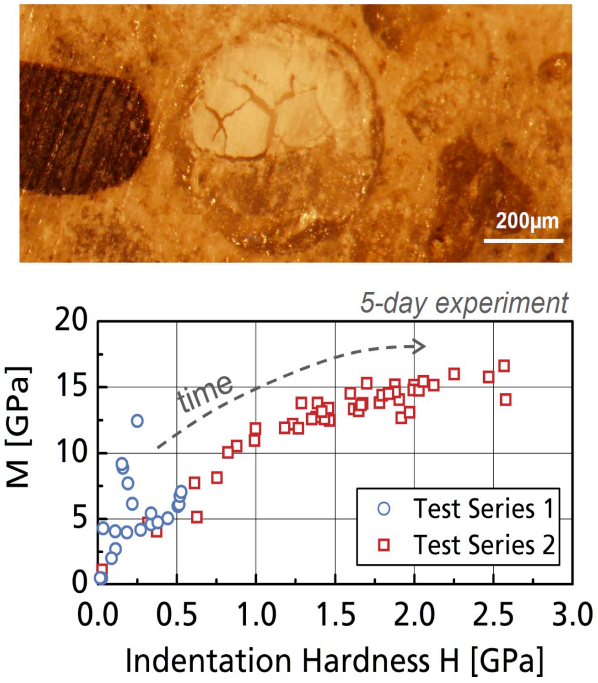

Figure 5 – (Top) Picture of an ASR gel region observed at the surface of a cross section of a mortar sample. (Bottom) Indentation modulus M vs hardness H of the ASR gel, determined over a time span of 5 days. The gel is drying and both M and H are increasing as water evaporates and the gels dries up.

mortar sample and exposing the ASR gel to ambient temperature and atmospheric pressure, nano-indentation does not allow to measure the gel mechanical properties, which are below the detection threshold of our equipment, showing that the sample is therefore too soft. One needs to wait several hours for the ASR gel to harden sufficiently due to drying, so as to display measurable mechanical properties. The lowest indentation modulus and hardness that we measure are respectively: $M_{min} \approx 400\ MPa$ and $H_{min} \approx 10\ MPa$, which are much lower values than that reported in the literature [3,4]. As time goes by, the ASR gel keeps drying as evidenced by the drift of both M and H towards larger values (figure 5, bottom). After 5 days exposed at relative humidity 50% to 60%, the gel sample displays much tougher mechanical properties, with terminal values $M_\infty \approx 15\ GPa$ and $H_\infty \approx 2.5\ GPa$. These results strongly suggest that ASR gel with native moisture content (i.e. saturated to 100% relative humidity) is weak and displays values of M and H that are much lower than the lowest values of M and H measurable by our experimental setup. In particular, ASR gel in saturated moisture conditions is much softer than the surrounding cementitious matrix for which $M > 10\ GPa$ and $H > 200\ MPa$ [6]. Our results highlight the key role played by the moisture content on the mechanical properties of ASR gels and raise the question of the true mechanical properties of ASR gel, in the limit of saturated moisture conditions.

In order to get more insights on the mechanical properties of ASR gels at controlled levels of relative humidity, we performed mechanical testing on lab synthesized ASR gels. The samples, which were provided by collaborators at Pennsylvania State University, display well-controlled chemical composition, and can be produced in batches sufficiently large to perform mechanical testing at the microscale [13]. These samples are prepared over liquid at 42% relative humidity, by mixing the chemical components in the desired proportions, before being cast into syringes sealed with high vacuum grease and shipped to MIT. Samples were opened and cored into cylinders (6 mm diameter) that were embedded in epoxy resin, before being stored at controlled humidity. Two types of samples were examined, mainly differing in their calcium content.

We first tested the impact of the relative humidity on the strength of the sample with the lowest calcium content (Ca/Si=0.1). Indentation tests, similar to that discussed above, show that the gel's strength is strongly sensitive to the relative humidity. Indeed, at relative humidity of 40%, the gel displays the following average indentation modulus and hardness: $M = (167 \pm 24)\ MPa$ and $H = (7.86 \pm 1.95)\ MPa$, whereas for a relative humidity of 75%, these values drop down to $M \approx 13\ MPa$ and $H \approx 78\ kPa$ respectively (see Figure 6)! Therefore, an increase of the relative humidity by a factor 2 results in a collapse of the gel's mechanical properties, by a factor 10 for the indentation

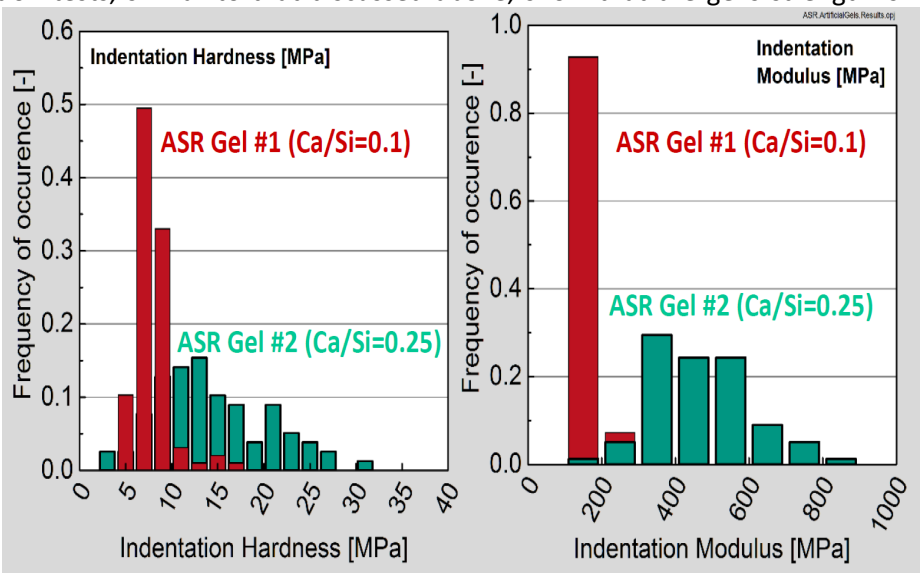

Figure 6 – Distribution of hardness H (left) and indentation modulus M (right) for two lab synthesized ASR gels, #1 (Ca/Si = 0.1) and #2 (Ca/Si = 0.25). Data obtained by microindentation (loading rate of 1.25 N/min, maximum load 0.15 N maintained for 180 s). Indentation grid of 10 x 10 = 100 indents.

modulus and a by a factor 100 for the hardness. From these measurements, one can extrapolate that in the limit of saturated moisture content, i.e. a relative humidity of 100%, ASR gels should display no hardness ($H = 0\ Pa$) and extremely soft mechanical properties ($M \leq 1\ MPa$), which indeed qualifies ASR gels to be referred to as gels! We emphasize that our indentation testing is only sensitive to the elastic component of the gel, whereas one should keep in mind that ASR gels most likely exhibit elastic and viscous properties due to their water content, which could be assessed by rheological measurements. Second, we have repeated the same type of indentation measurements on a second lab synthesized ASR gel (Figure 6), with a different chemical composition, i.e. a higher calcium content (Ca/Si = 0.25) than the first gel (Ca/Si = 0.1). All things being equal, at 40% relative humidity, the gel with higher calcium content exhibits tougher mechanical properties characterized by a broader distribution: $M = (467 \pm 200)\ MPa$ and $H = (14.3 \pm 6.0)\ MPa$ (dispersion of about 40% vs 15 to 25% for the gel with a lower calcium content). This result shows that the presence of calcium leads to stronger gels.

To conclude, we have shown that the moisture content of ASR gel is a key controlling parameter of its mechanical properties. Experimental results on both natural and synthesized gels show that the mechanical strength of ASR gels decreases with increasing moisture content. Extrapolating from our results, we can safely suggest that the hardness of the gel vanishes in the limit of saturated water content, and that therefore, in situ ASR gels behave as soft viscoelastic materials with negligible strength compared to the surrounding cementitious matrix.

3.1.2 Experiments of temperature impacts on rate of expansion

Due to the non-linear expansion associated with ASR (see Figure 7), a kinetic-type performance model (equation 1) is used to characterize expansion behavior. Expansion associated with ASR, has been known to result in initial aggregate dissolution followed by gel formation, which can be referred to as the characteristic time and latency time (beyond ε_i in Figure 7), respectively. By fitting this model to the measured expansion data over time, the parameters (ε, β, t_0, ρ) can be calculated.

$$\frac{1}{\varepsilon} = \frac{1}{\varepsilon_0} e^{\left(\frac{\rho}{t-t_0}\right)^{\beta}} \quad (1)$$

where:
ε_0 = ASR ultimate expansion
β = rate constant
t_0 = initial time of ASR expansion (hr)
ρ = time corresponding to an expansion (ε_0 / ε)

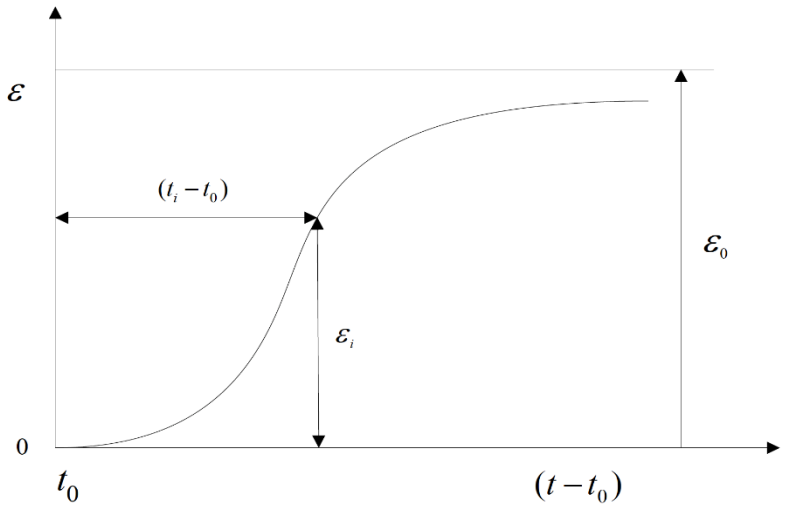

Figure 7 – Common behavior of ASR expansion

The evaluation of the β parameter (equivalent to rate constant) can be determined using equation 1, which can be transported into a linear form by taking the double natural logarithm as presented in equation 2.

$$ln\left[-\ln\left(\frac{\varepsilon}{\varepsilon_0}\right)\right] = \beta ln \propto -\beta \ln\left(t - t_0\right) \qquad (2)$$

The rate constant (β) can then be determined from the slope of the regression line (as seen in Figure 8) by plotting the relationship between ln[-ln(ε- ε_0)] and ln(t-t_0).

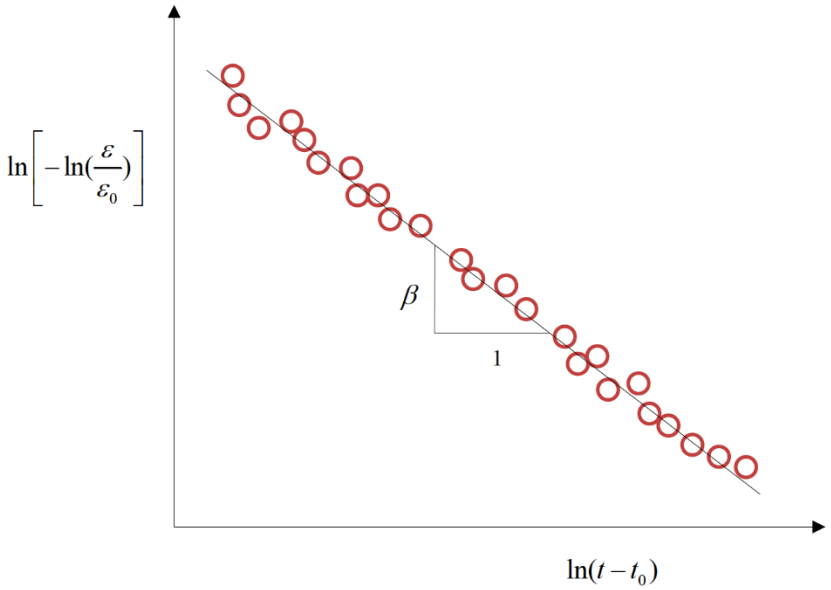

Figure 8 – Relationship between ln[-ln(ε- ε0)] and ln(t-t0)

The rate constant values at multiple temperatures (minimum of three) are then determined and the activation energy is calculated by plotting ln(β) versus (1/T) (see Figure 9). The slope of the linear regression is equal to (-E_a/R), where R is the universal gas constant and E_a is the activation energy. In analytical chemistry, activation energy (E_a) is defined as the minimum energy required for a chemical reaction to proceed, however, for ASR, it can be considered to be the minimum energy required to initiate expansion taking into account the combined effects of time, temperature and alkalinity (see Figure 9).

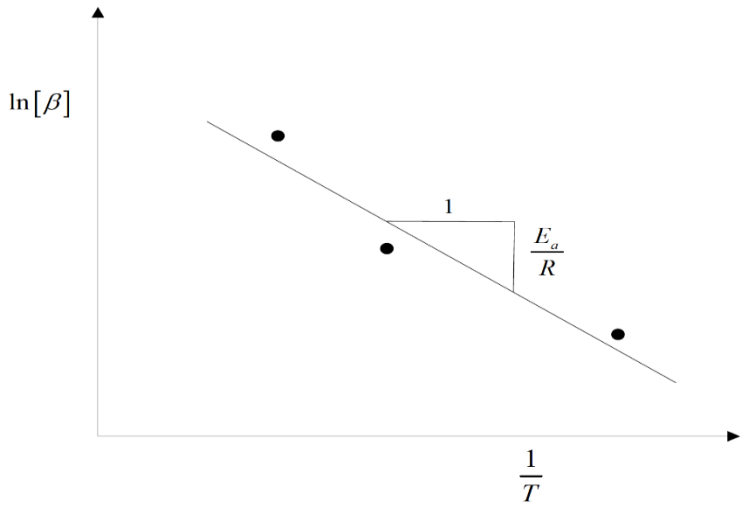

Figure 9 – Determination of activation energy

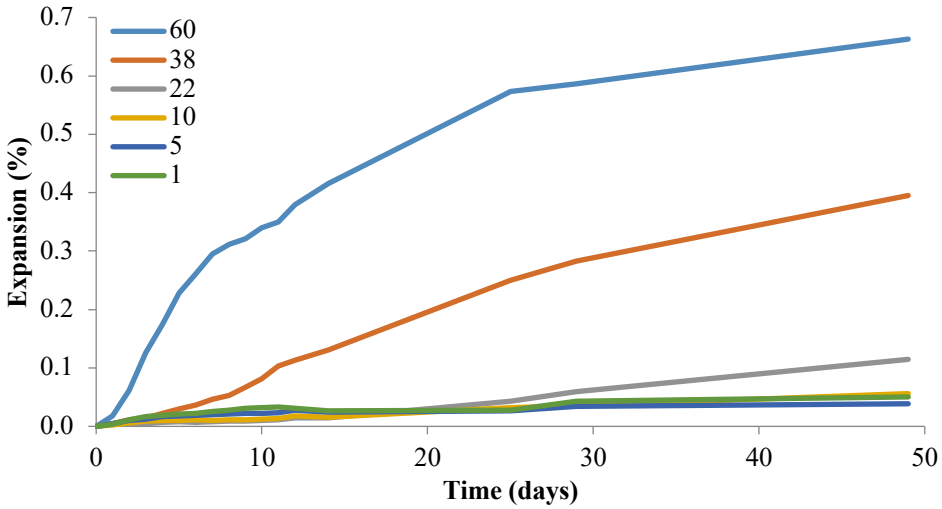

Figure 10 – Expansion relative to exposure temperature

In order to determine the activation energy of a single aggregate, mortar prisms (1 x 1 x 11.5 in.) were cast and cured in accordance with ASTM C1260. All specimens were cast using a reactive Jobe aggregate from El Paso, Texas. Jobe is regarded as a highly reactive aggregate in accordance with ASTM C1778. Following initial curing and zero day readings, specimens were placed in a container with sufficient 1N NaOH solution at a range of temperatures (1, 5, 10, 23, 38, and 60°C [34, 41, 50, 73, 100, 140°F]). Length change was then measured on a daily basis until 14 days in order to observe the characteristic time after which they are currently being measured on a bi-weekly basis. The average expansion of three prisms exposed to a range of temperatures is presented in Figure 10. Additional long-term expansion data is needed to determine the activation energy as a result of the slower reactive time at lower temperatures.

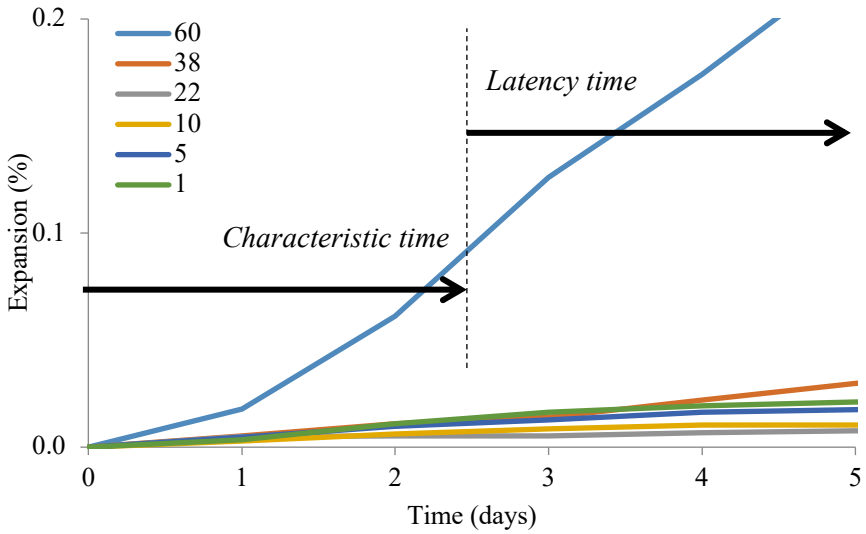

Figure 11 – Characteristic and latency time of prisms exposed to 60°C (140°F). Colored lines refer to different temperatures for experiments.

However, the boundary between characteristic and latency times of prisms exposed to 60°C is presented in Figure 11 as a result of the change in slope similar to that presented in Figure 7.

3.1.3 Validation experiments on alkali-induced C-S-H swelling

Since its discovery, damage as a result of alkali-silica reaction has been attributed to the expansion of concrete as a result of deleterious alkali-silica gel. However, by studying sodium and calcium contents of individual components (C-S-H and ASR gel), it was hypothesized that the driving-force of the swelling may be attributed to C-S-H and not expanding siliceous gel. As a result, a test program was initiated at the University of New Brunswick to validate this theory by casting mortar mixtures with varying amounts of calcium hydroxide (CH) and C-S-H in order to study its effect on ASR. Mortar prisms (1 x 1 x 12") were cast in accordance with ASTM C227, using cementitious materials presented in Table 1 with both a highly reactive fine aggregate from El Paso, Texas or a non-reactive EN-196 sand. All prisms were cured for 28 days in lime-water at 38°C (100°F) after which they were submerged in a 0.5 M NaOH + 0.5M KOH solution at 38°C (100°F) where they were measured for length change periodically. Table 1 presents a list of mixtures studied in order to study the effect of hydration products. Cementitious materials and proportions were selected in order to study the effect on varying levels of both C-S-H and CH and how they might affect ASR. Figure 12 presents the expansion of various mixtures up to approximately 350 days. To date, only binders with C-S-H, CH and reactive aggregate (Jobe) have expanded (i.e. PC (JB)). Mixtures containing significant amounts of C-S-H and non-reactive EN-196 sand show no signs of expansion (i.e. PC+FA (JB)).

Also, binders with no CH and reactive aggregate do not expand, regardless of the presence or composition of C-S-H. In addition to mortar mixtures, the performance of portland cement paste specimens exposed to 5M NaOH solution is also presented. The inability for this system to expand under such a high alkaline environment, disproves the theory that C-S-H is the sole cause of ASR expansion.

Table 1 – Cementitious materials and hydration products

Cementitious material	Hydration product(s)
Portland cement (Na_2Oeq = 0.92%)	C-S-H, CH
Alkali-Activated Fly Ash	no C-S-H, no CH
Calcium Sulfoaluminate Cement	AFt, small amount of C-S-H, no CH
Calcium aluminate cement (CAC)	no C-S-H, no CH
CAC + calcium hydroxide	CH, CAH
Carbonated portland cement	No C-S-H, no CH, CC
PC + 30% Silica Fume	C-S-H
PC + 70% Fly Ash	C-S-H
SF + CH (1:1, 1:2, 1:3, 3:1, 2:1)	C-S-H

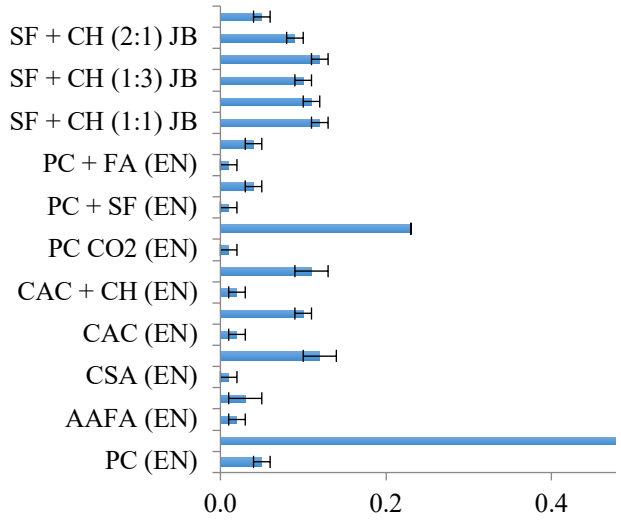

Figure 12 – Expansion of mortar and paste specimens following 350 days

3.2 Modeling investigation of ASR mechanisms

As explained above, there are unresolved issues as to the mechanistic origins of ASR. The CSHub team set out to clarify and verify these hypotheses and assumptions using atomistic and mesoscale modeling. In particular, the effort focused on the effect of elevated local concentrations of alkali ions on C-S-H. Recent CSHub-based scanning electron microscopy by Krakowiak et al. ( ) demonstrated that the C-S-H matrix in proximity of ASR gel veins was rich in alkali ions (see Figure 13). The presence of an elevated concentration of alkali ions in the vicinity of the C-S-H grains could lead to sorption of alkali by the C-S-H and modification of its properties.

In typical silica glasses, sorption of alkali ions leads to expansion. The CSHub's working hypothesis was that such an alkali-induced expansion was taking place in the C-S-H interlayer. For this to take place, a few questions needed to be clarified:

1 - Do alkali ions adsorb at the surface of C-S-H grains, or in their interlayer?

2 - At what rate does sorption take place?

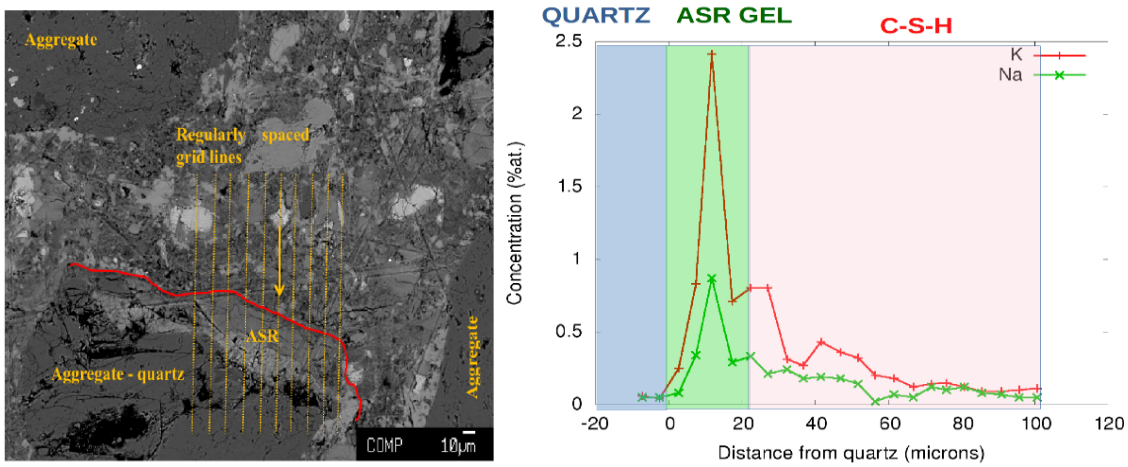

Figure 13 – Scanning electron microscopy evidence of elevated alkali concentration in the C-S-H matrix within tens of microns away from an ASR vein.

3 - What are the effects of alkali sorption in the interlayer on the size and mechanical properties of the C-S-H particles?

4 - Do these changes in size and mechanical properties of the C-S-H nanoparticles—if any—lead to significant swelling pressure, averaged over hundreds of nanometers?

5- How do the ASR gels form in the pores?

The CSHub team was able to leverage its existing nanoscale and mesoscale models of C-S-H to answer these questions, by coupling them to a number of state-of-the-art simulations methods. An illustration of the nanoscale and mesoscale models used is presented in Figure 14.

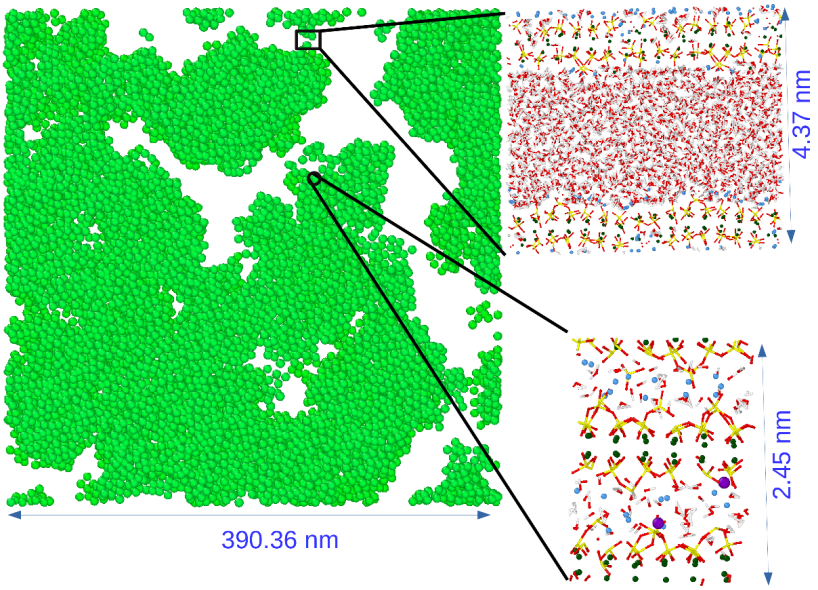

Figure 14 – An illustration of the multi-scale approach employed by the CSHub. We can see Ioannidou et al.'s mesoscale model (left), and Bonneau et al.'s atomistic pore surface model (top right) and Qomi et al.'s atomistic C-S-H model (down right).

1 - Do alkali ions adsorb at the surface of C-S-H grains, or in their interlayer? In order to answer this question, we compared the energetics of binding alkali ions at the pore-facing surface of a C-S-H grain to the energetics of binding alkali-ions in the interlayer of the grain. More specifically, a semi-grand canonical Monte Carlo procedure was designed to simulate adsorption in the interlayer. The idea is that the system was allowed to swap Ca^{2+} ions for 2 Na^{+} or K^{+} ions. The propensity of the system to encourage this swap is determined by the differences in chemical potential of the Ca2+ ions and Na+/K+ ions. This difference in chemical potential can be estimated using atomic binding energies from molecular dynamics simulations of sorption at the pore-facing surface of the grain, at different ionic concentrations. Adsorption isotherms in the interlayer were computed (see Figure 15a for an example of a C-S-H grain loading up with K+) and revealed two important results: (i) alkali ion sorption takes place preferentially in the interlayer, at ionic concentrations lower than about 0.05 mol/kg and takes place preferentially at the pore surface at higher ionic concentrations; and (ii) alkali ion adsorption in the interlayer is favored at low Ca/Si ratio. For reference, typical alkali ion concentration in C-S-H is of the order of 0.02 mol/kg, reaching up to ~0.2 mol/kg in the vicinity of ASR gels, and Portland cement has a typical Ca/Si ratio of 1.8, which is on the high-end of the C-S-H compositions studied here (1.0 to 2.0 Ca/Si ratios).

2 - At what rate does sorption take place? We can infer from diffusion experiments in various silica glasses and minerals that diffusion of alkali ions in C-S-H is a slow process, outside the range of conventional molecular dynamics simulations. In order to estimate the diffusion timescales, the CSHub team implemented an algorithm based on the Activation Relaxation Technique nouveau, which is itself founded on transition state theory. This method directly explores the potential energy landscape of the system, and handles atomic vibrations using statistical mechanics, rather than explicitly simulating them, as would be done in molecular dynamics. Thousands of kinetic trajectories were generated in all our 150 atomistic C-S-H models. One example is illustrated in Figure 15b. It was found that the overall barrier to diffusion of the ions is lower than 1 eV, and that diffusion times at room temperatures are of the order of several nanometers per hour. In other words, alkali ions can enter the C-S-H interlayer and adsorb within a few hours.

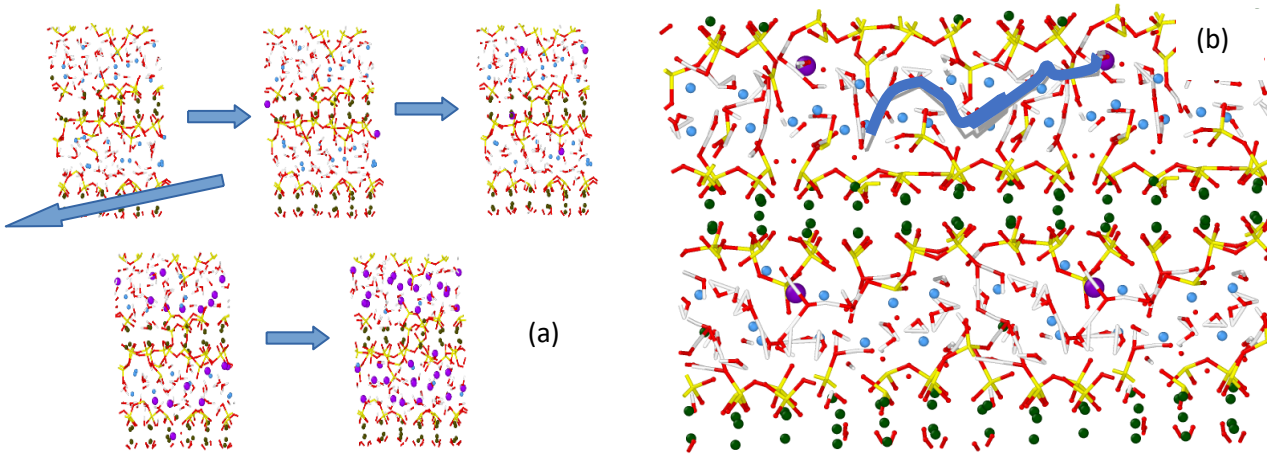

Figure 15: (a) A C-S-H interlayer being loaded by potassium, as calculated by our semi-grand canonical Monte Carlo procedure. (b) A potassium ion trajectory in C-S-H. The ion takes about 5 hours to diffuse over 1.5 nm.

3 - *What are the effect of alkali sorption in the interlayer on the size and mechanical properties of the C-S-H particles?* In order to answer Question 1, above, the CSHub team generated C-S-H configurations loaded with Na and K. The mechanical properties of these alkali-rich C-S-H grains were calculated. While the bulk and shear moduli of the grains are not significantly affected by uptake of 0.05 mol/kg Na+ or K+, there

was a noted volume expansion of the grains. In some cases, the model simulated volume expansion on the order of 1 percent.

4 - Do these changes in size and mechanical properties of the C-S-H nanoparticles—if any—lead to significant swelling pressure, averaged over hundreds of nanometers? To answer this question, a mesoscale model of C-S-H was needed. For this purpose, the model developed by Katerina Ioannidou — i.e. the CSHub model — was employed. Because high concentrations of alkali ions might be present in the pores, we performed supplementary potential mean force calculations in order to correct the interaction between C-S-H grains. We tested the mesoscale mechanical performance of the model when grains undergo alkali-induced expansion. We considered scenarios that involve low and high ion concentration in the pore solution, and expansion of either all grains, or solely of grains in contact with capillary pores. Under most scenarios, the mesoscopic structure can accommodate the grain expansion with little to no residual expansive pressure. In other words, while high local concentration of alkali leads to expansion of the C-S-H grains, it does not generate enough expansive pressure to explain ASR expansion of concrete.

5 - How do the ASR gels form in the pores? To answer this question, we used state-of-the-art atomistic simulations to overcome the time-scale issue. We coupled parallel tempering molecular dynamics to accelerate the dynamics with GCMC method to account for the wet environment inside the pores. As the silicate chains are formed, our model is able to add or remove water molecules. Using a reactive force field (Reaxff), were able to simulate the formation of ASR gels starting from liquid configurations with different compositions (see Figure 16).

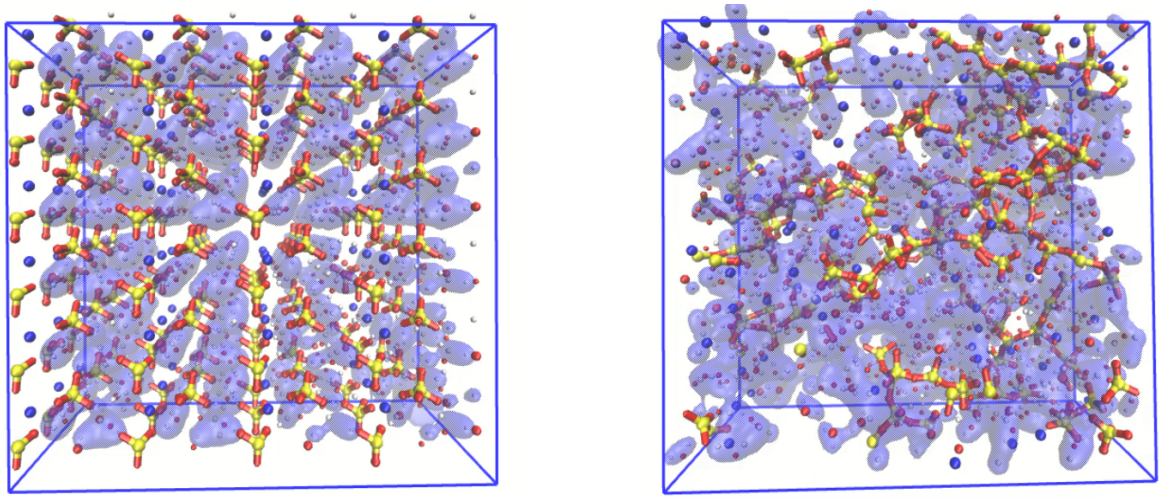

Figure 16 – Snapshots of the simulation. Silicon atoms are in yellow, blue spheres represent the cations, water molecules are represented by transparent pale blue volume. (left) initial "liquid" configuration with only silica monomers Q_0. (right) structure after the simulation that contains silicate chains of various length.

The final structure is formed by silicate chains of various length. Silicon atoms are mostly in Q2 and Q3 positions but also Q4 positions are observed corresponding to the local formation of glass, as observed in NMR experiments*. We observe that water molecules and the silicate structure partially de-mix* (see Figure 16)*. These structures can now* be used to define the effect of sodium or potassium ions' replacement by calcium on the volume and elastic gel properties.

3.3 Synthesis: what causes the expansive pressure in ASR-affected concrete?

Combining the knowledge gained from experiments run at MIT and UNB together with multiscale simulation results carried out at MIT, we are now in a position to clarify several key points and propose a realistic scenario for ASR in accordance with all experimental facts. First, for ASR damage to occur, four ingredients are required: (i) a large degree of water saturation, (ii) the formation of an alkali silica gel, (iii) the calcification of ASR gel over time, and (iv) time: ASR is a slow process that can take place at the scale of decades after concrete/cement setting. Here are key findings from the work coordinated by the CSHub@MIT and CNRS in collaboration with UNB and PSU.

- When containing a large amount of water, the ASR gels have no or very little mechanical properties and are unlikely to damage a cement hydrate matrix in concrete. So at large degree of water saturation of the cement paste porosity (> 80%), an ASR gel *per se* (produced by the surface dissolution of aggregates in a concrete mix) cannot exert significant mechanical pressure. Upon drying an ASR gel starts gaining rigidity and exhibits mechanical properties asymptotically reaching those of silica glasses with equivalent alkali content. An increasing content of calcium in an ASR gel also tends to rigidify an ASR gel. Nanoindentation experiments showed a clear demonstration of the role of the water and calcium contents in ASR gels mechanical properties.

- The assumption that it could be a Na → Ca exchange was confirmed from SEM microscopy showing that the alkali concentration around an ASR vein extends well (several microns) into the surrounding C-S-H matrix. Calcium hydroxide is shown to be the main source of calcium for the Na → Ca exchange with the ASR gel. Molecular simulations of alkali intake in C-S-H (one pristine Ca2+ ion in C-S-H being substituted by 2 Na+) shows that this is thermodynamically possible (at room temperature) and is most probable for low Ca/Si C-S-H (Ca/Si = 1); indicating that for the most common C-S-H in a cement paste with Ca/Si=1.7, alkali intake is actually small.

- Molecular simulations also indicate that the increase of calcium content in a pristine ASR (sodium) gel by the substitution of 2 Na+ by 1 Ca2+, contracts the gel while it rigidifies, in agreement with nanoindentation experiments. Hence an “old” gel that gets more rigid upon Ca intake is not “swelling” and cannot damage the surrounding C-S-H matrix. This is clearly a new result that sheds new light on the ASR mechanism. In summary, a fresh ASR gel has no mechanical properties *per se* and is therefore unlikely to cause any damage to the C-S-H matrix. On the other hand, an older gel that has gotten richer in calcium because of some Na → Ca exchange mechanism cannot cause any direct damage to the same C-S-H surrounding matrix as it shrinks. Note that the alkali-silica gel developed at early age is generated by reactive aggregate such as Jobe, as demonstrated in the present report. Macroscopic experiments on the ASR mortar bars here reported in the present document also show that the Na → Ca exchange mechanism is based on calcium species provided by CH..

- Coarse grained mesoscale simulations in a primitive model one-plasma component approach of statistical physics reveal that the interactions between the ionic species (especially alkali) confined in a nanometer-thick wetting layer in-between the charged surface of C-S-H and the neutral (or quasi-neutral) surface of the calcium-rich (rigid) ASR gel create an osmotic disjoining pressure. A key finding of this work was to demonstrate that this ionic disjoining pressure at the C-S-H/ASR gel interface due to a wetting confined alkali-rich electrolyte can reach pressure that can exceed C-S-H matrix strength and cause damage.

In conclusion, by combining mechanical and characterization experiments together with atomistic and mesoscale simulations, we found that there is no direct effect of ASR swelling gel making the C-S-H matrix

crack. ASR damage appears to be the consequence of a Na←→ Ca exchange mechanism between an early-age alkali-silica gel produced by the reactive concrete aggregates and cement hydration products over time that creates a disjoining ionic pressure at the C-S-H/calcified (calcium rich) alkali-silica gel interface in the capillary porous network of C-S-H, which is able to fracture the C-S-H matrix. This requires the presence of an interfacial nanometers-thick electrolyte layer.

3.4 Mitigation: what can we do to avoid ASR damage?

Having suggested the key role of an alkali-rich nanometers-thick electrolyte layer at the C-S-H/ASR gel interface in creating a disjoining pressure large enough to exceed C-S-H matrix strength, we are in a good position to propose a sound mitigation strategy. First this pressure finds its origin in the existence of ions able to move in a nanometer-thick interfacial water layer at the C-S-H/capillary pore surface. Removing this water will prevent any ionic movements and hence will suppress the ionic disjoining pressure between C-S-H and Ca-rich/but contracting ASR gel. In other words, making C-S-H pores hydrophobic is a potential strategy to mitigate ASR.

We propose to dope cement hydrate paste with carbon black or porous carbon. We found that with a carbon / (binder + water) ratio around 5% produces a black cement paste that has the property of conducting electrons like a piece of metal thanks to a percolative network of carbon black nanoparticles (characteristic size: 200 nm) confined to the large capillary pores of the cement paste. This hydrophobic substance in the cement paste will naturally reduce the amount of water in the capillary pores. Besides electrical conductivity, carbon-doped cement paste also exhibits an interesting Joule effect: the polarization of a 2 cm^3 cylinder of “black cement” with a few volts enables an increase of the external sample surface up to 100°C with respect to the ambient room temperature. This effect vaporizes water and hence reduces the water content in the cement paste capillary pores, which reduces/removes any ASR-related ionic disjoining pressure.

References

[1] Alnaggar, M., Cusatis, G. and Di Luzio, G., 2013. Lattice discrete particle modeling (LDPM) of alkali silica reaction (ASR) deterioration of concrete structures. *Cement and Concrete Composites*, *41*, pp.45-59.

[2] Alnaggar, M., Di Luzio, G. and Cusatis, G., 2017. Modeling Time-Dependent Behavior of Concrete Affected by Alkali Silica Reaction in Variable Environmental Conditions. *Materials*, *10*(5), p.471.

[3] Bažant, Z.P. and Rahimi-Aghdam, S., 2016. Diffusion-Controlled and Creep-Mitigated ASR Damage via Microplane Model. I: Mass Concrete. *Journal of Engineering Mechanics*, *143*(2).

[4] Charpin, L., 2013. *Modèle micromécanique pour l'étude de l'anisotropie de la réaction alcali-silice* (Doctoral dissertation, Université Paris-Est).

[5] Dunant, C.F. and Scrivener, K.L., 2016. Physically based models to study the alkali–silica reaction. *Proceedings of the Institution of Civil Engineers-Construction Materials*, *169*(3), pp.136-144.

[6] Ichikawa, T. and Miura, M., 2007. Modified model of alkali-silica reaction. *Cement and Concrete research*, *37*(9), pp.1291-1297.

[7] Liaudat, J., LÓPEZ, C.M. and Carol, I., 2016. Numerical and experimental study of ASR in concrete at the meso-level. In *9th International Conference on Fracture Mechanics of Concrete and Concrete Structures: full papers* (pp. 1-11).

[8] Leemann, A. and Lura, P., 2013. E-modulus of the alkali–silica-reaction product determined by micro-indentation. *Construction and Building Materials*, *44*, pp.221-227.

[9] Multon, S., Sellier, A. and Cyr, M., 2009. Chemo–mechanical modeling for prediction of alkali silica reaction (ASR) expansion. *Cement and Concrete Research*, *39*(6), pp.490-500.
[10] Vayghan, A.G., Rajabipour, F. and Rosenberger, J.L., 2016. Composition–rheology relationships in alkali–silica reaction gels and the impact on the Gel's deleterious behavior. *Cement and Concrete Research*, *83*, pp.45-56.
[11] Ulm, F.J., Coussy, O., Kefei, L. and Larive, C., 2000. Thermo-chemo-mechanics of ASR expansion in concrete structures. *Journal of engineering mechanics*, *126*(3), pp.233-242.
[12] F. Rajabipour, E. Giannini, C. Dunant, J.H. Ideker and M.D.A. Thomas, *Cem. Conc. Res* **76**, 130 (2015)
[13] A. Gholizadeh Vayghan, F. Rajabipour and J. L. Rosenberger, *Cem. Conc. Res.* **83**, 45–56 (2016)
[14] A. Leemann and P. Lura, *Construction and Building Materials* **44**, 221–227 (2013)
[15] C.V. Johnson, J. Chen, N.P. Hasparyk, P.J.M. Monteiro and A.T. Akono, *Cement and Concrete Composites* **79,** 71–75 (2017)
[16] W.C. Oliver and G.M. Pharr, Journal of Materials Research **19**, 3-20 (2004)
[17] F.-J. Ulm, M. Vandamme, C. Bobko, J.A. Ortega, K. Tai and C. Ortiz, Journal of the American Ceramic Society **90**, 2677–2692 (2007)
[18] L. Struble and S. Diamond, Journal of the American Ceramic Society, **64**, 652 – 656 (1981)

4 Freeze-thaw damage

A number of potential mechanisms responsible for freeze-thaw (FT) have been proposed, and they can generally be classified as in one of two categories: (i) classic freeze-thaw damage due to formation of ice when concrete is at a saturation level greater than a critical level., and (ii) chemical reactions between deicing chloride-bearing salts (especially $CaCl_2$ and $MgCl_2$ and the cementitious matrix, with calcium hydroxide, $Ca(OH)_2$). Recent research has described how pavements can be designed to resist deicer salt damage [1-9]. The focus of this chapter is the impact of degree of saturation on ice formation damage [10-12] and the source of pressure that causes FT damage. We present some methods to better study the effect of degree of saturation, followed by experimental and modeling investigations into the chemistry and mechanics of FT damage. We conclude with a discussion of the research results and a summary of methods to mitigate FT damage.

4.1 Saturation-based freeze-thaw model

While there are many thoughts on classic freeze thaw mechanisms, Figure 17 describes a sorption-based model for reaching a critical degree of saturation [10, 13-15]. Fagerlund (1977) pioneered the use of this sorption-based approach and suggested that concrete would not be able to withstand freezing when saturation levels exceed a certain critical level of saturation based on the volume change of water to ice, this was postulated as 91% of the porosity. This value has been measured to be 86% for air-entrained concrete mixtures representative used for typical concrete pavements [10], but can vary from 78% to 91% [14] based on other concrete properties, such as air void spacing and air content (note in general smaller and more uniformly spaced air corresponds to a higher critical degree of saturation). The critical degree of saturation will be assumed to be 85% for the examples discussed in this document.

Bentz et al. [16] modified and used the sorption-based approach to predict freeze-thaw damage in concrete pavements. To better understand the sorption terms in this model Lucero et al. [17] used neutron radiography to examine the relationship between the initial rate of absorption and pores that were being filled, proposing that the initial absorption (shown in brown in Figure 17) corresponds to the filling of gel and capillary pores while the secondary rate of sorption (shown in blue in Figure 17) was related to the filling of larger pores like air voids. It should be noted that the original moisture state of the concrete impacts the y-intercept of this graph. If the concrete is more dry the initial degree of saturation is lower and the gel and capillary pores fill. However if the concrete has a higher initial degree of saturation some of these pores begin filled. For example, the gel pores will be filled when the relative humidity of the sample is greater than 80%. The findings from Lucero et al. [15] have indicated that the transition between the initial absorption and secondary absorption (commonly referred to as the nick point) can be described by the degree of saturation that

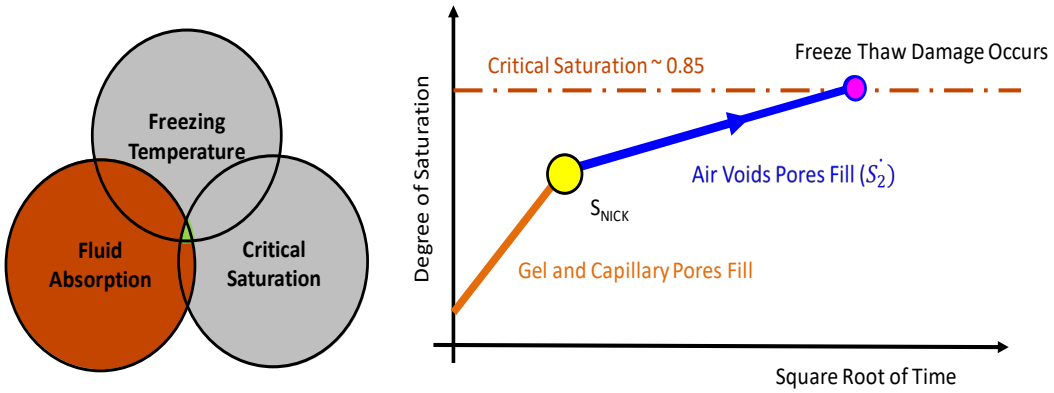

Figure 47: A conceptual illustration of the sorption-based model

fills in all the pores in a concrete with the exception of the air voids (this would include the gel and capillary pores). The Powers-Brownyard model [18] can be used to determine the degree of saturation at the nick point for different water to cement contents, degrees of hydration and air contents. This degree of saturation is also a function of the entrained air volume [19] (see Figure 18a). It can be noticed that concrete with more air has a lower degree of saturation initially (i.e., is further away from reaching critical saturation). More recent research has focused on extending the Powers-Brownyard model to a thermodynamics based model that uses Gibbs Energy Minimization Software (GEMS) to enable a wider range of material chemistries to be used (i.e., concretes with supplementary cementitious materials) [20, 21]. While the extension of the Powers-Brownyard model is in its infancy (i.e., coupling the GEMS modeling with the Pore Portioning Model for concrete, PPMC), this approach shows substantial promise [20, 22-24]. Since experiments have shown that when water is in contact with concrete (a 50-mm thick sample was used) the nick point will generally be reached during the first 24 hours [17], the prediction of service life for concrete pavements would not need to consider the initial absorption and the prediction can begin assuming that the matrix is saturated (i.e., S_{NICK}). With this assumption, the secondary rate of sorption can be used to predict the time required to reach the critical degree of saturation (t) as shown in Eq. 3:

$$S_{CR} = S_{NICK} + \Delta S\sqrt{t} \tag{3}$$

where, S_{CR} is the critical degree of saturation, S_{NICK} is the degree of saturation between the initial and secondary absorption which occurs when all the pores except the air voids are filled, ΔS is the secondary rate of sorption and t is time. Entrained air improves freeze-thaw durability by reducing the degree of saturation in concrete [25]. Air entraining admixtures stabilize air bubbles generated during mixing to add small (approximately 0.05 to 1.25 mm), stable, air-filled voids to the paste portion of the concrete [26]. These air filled voids reduce the initial degree of saturation [19] as shown in Figure 18a. This graph indicates that a 1% change in the volume of air will have approximately a 5% reduction in the degree of saturation at the nick point (S_{NICK}). Figure 18b illustrates that as the volume of air increases the time to reach critical saturation (which can be assumed to be time of damage initiation). Increasing the air content will extend the life of the concrete by increasing the time required to critically saturate the concrete. Some may argue however that at some point the addition of air results in a decrease in compressive strength and there are limited benefits of increasing the freeze-thaw resistance of a concrete that is already freeze-thaw resistant.

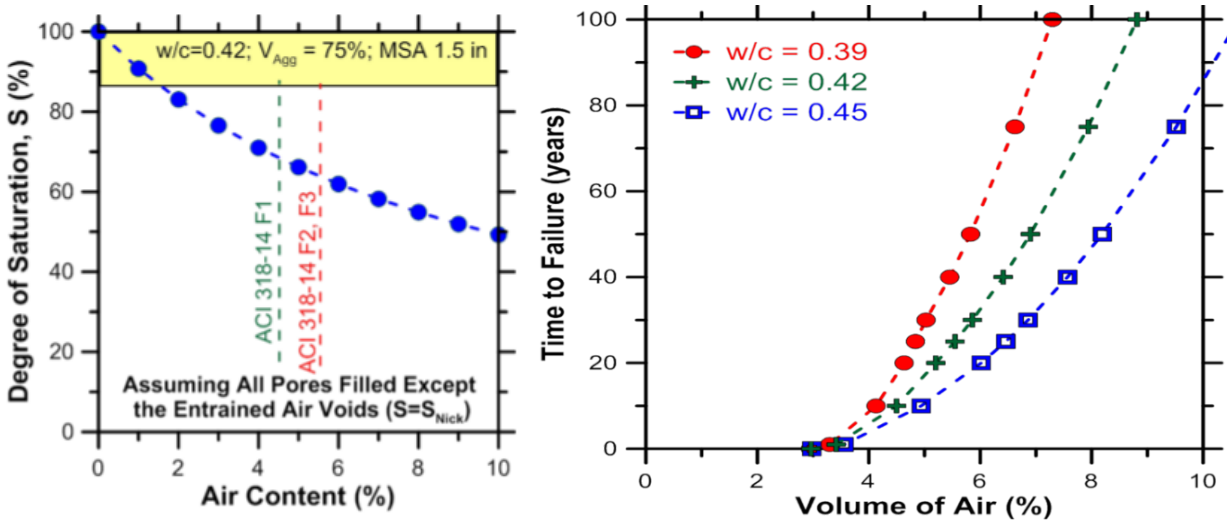

Figure 18: (a) The influence of air content on the initial degree of saturation and (b) the influence of air content on the time to reach critical saturation

Further, increasing the air content will provide additional greater volume of air voids, which can accommodate the formation of deleterious phases while also enabling the air to function as entrained air in a partially saturated system [19]. The basic FT process begins with air voids filling, which creates pressure, which leads to damage. Two existing theories on the source of the pressure are listed followed by a newer theory proposed here.

4.1.1 Hydraulic Pressure Theory

Water expands 9% by volume during freezing and it is currently understood that this volume change causes movement of water within concrete pores and is the source of hydraulic pressure inducing damage in cement paste. When the pores are critically saturated, hydraulic pressure is generated [52]. When the pressure exceeds the tensile strength of concrete, cracking occurs. Powers and his coworkers [53] also noticed that the freezing rate influenced the damage mechanisms. It is commonly believed that hydraulic pressure governs the freezing deterioration at a fast freezing rate and induces cracks in the matrix. This somewhat pictures the C-S-H matrix as made of closed, unconnected pores. Our X-ray tomography experiments (35 × 35 × 65 μm3 with a pixel size resolution of 64 nm) obtained in collaboration with the CEREGE laboratory (CNRS and Aix-Marseille University) and carried out on ordinary portland cement paste with w/c=0.42 cured at 28+ days reveal that in fact that the capillary pores system in C-S-H is highly connected (>92%). Figure 19a shows the network of the capillary pores system in C-S-H. This suggests that entrained air bubbles are buffers where water is displaced to upon freezing conditions as shown by Monteiro et al. [51], see Figure 20. It is important to note that the hydraulic pressure theory for FT damage in cement/concrete not only ignores capillary pores' connectivity in the cement paste, but also assumes a direct contact between ice and C-S-H ignoring the existence of a non-freezing nanometers-thick water layer as the surface of all capillary pores even in freezing conditions..

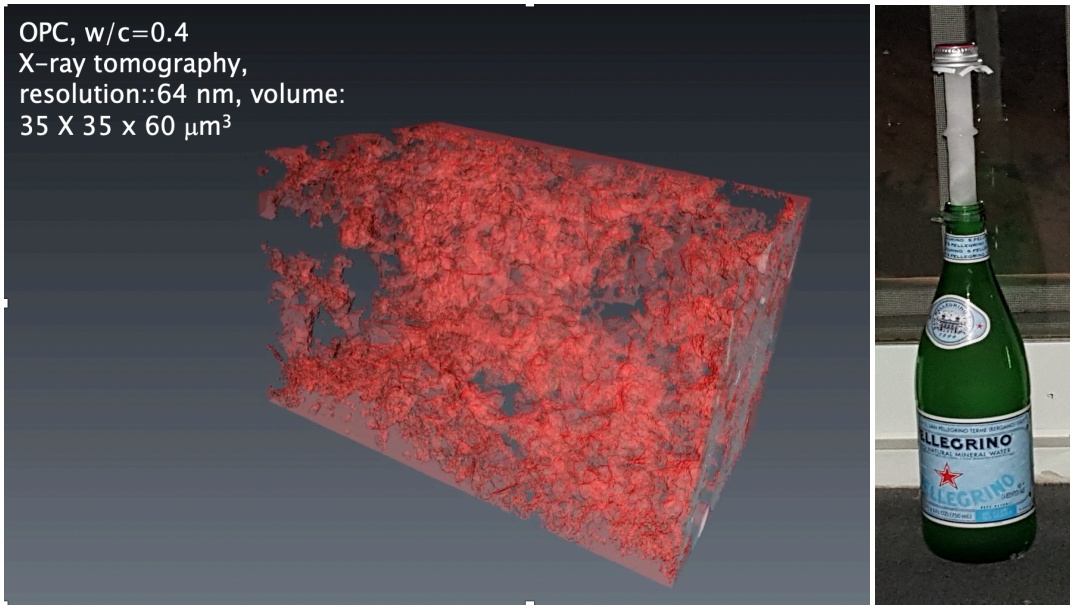

Figure 19: (a) X-ray tomography of C-S-H OPC with w/c=0.42 cured at 28+ days (carried out at CEREGE, CNRS/AMU, France), (b) the growth of an ice grain/cap perpendicular to the direction of main confinement indicating that in the case of a connected pore network represented by the bottle body + its neck, ice can invade the porosity without exerting pressure on the pore walls (note that the bottle body remains transparent i.e. filled with liquid water)

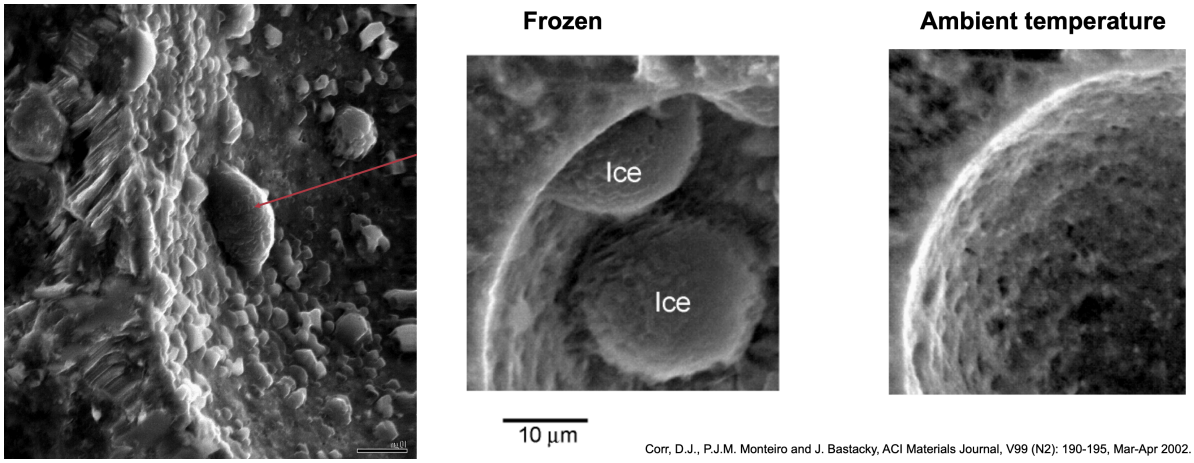

Figure 20: SEM image of the interior of an air-entrained bubble that host water ice grains indicating that the water is first displaced to these air bubble regions upon freezing conditions

4.1.2 Osmotic Pressure Theory

During freezing, water was found to diffuse toward, not away from, the sites of freezing. This is contrary to the hydraulic pressure theory. Powers attributed this phenomenon to osmotic pressure [54]. The water in concrete pores contains some dissolved ions and salts, which causes an initial super-cooling. As temperature drops to its freezing point, ice crystals will form in the larger capillaries, thus increasing the ionic concentration of the unfrozen solution near the freezing sites, which raises the osmotic potential of the unfrozen solution causing water to be drawn from surrounding smaller pores toward the freezing sites. This dilutes the solution surrounding ice allowing further growth of the ice body. When the pores are filled with ice and solution, any further osmotic flow of water causes a pressure buildup [52]. The prime location of this unfrozen solution is the non-freezing nanometers-thick water layer at the surface

of all capillary pores even at full saturation in freezing conditions. Indeed, the ion concentration in this layer increases upon freezing as the ice crystals forming in the capillary pores reject all ion in this liquid interfacial layer. This leads us to postulate the existence of the building-up of a disjoining ionic pressure in this interfacial region (here between the charged surface of C-S-H and the almost uncharged surface of ice crystals in the capillary pores). The disjoining ionic pressure will be transmitted to the C-S-H matrix only if the growing ice phase can withstand this pressure, i.e. when the temperature is cold enough. Experimentally, temperature of -7 °C (20 °F) is reported has being the critical value for which damage in concrete is observed). Furthermore, it is well documented that FT can be aggravated by the use of deicing agents, alkali salts being more detrimental than alkaline-earth salts for slab/pavement durability. From the work presented in the present report in collaboration between OSU and MIT, it is clear that FT is primarily related to ionic concentration in capillary pores. Ionic activity can only develop at high levels of saturation of the pore network portrayed in Figure 21a. Ionic activity and large water content are the key elements to explain FT. It is therefore natural to describe FT within the same theoretical frame as ASR i.e. the solidification of a phase in capillary pores hard/stiff enough to stand an ionic disjoining pressure that develops in the nanometers-thick solution layer at the interface between C-S-H and this growing solid phase (cold enough ice or ASR-Ca-rich gel). We believe that this theoretical frame can be extend to any confined solidification processes.

4.1.3 Proposed Theory

- The process is crystallization in a porous medium (cement paste, concrete) due to drop of temperature.

- The necessary conditions that can lead to damage are:
    a. water saturation (DS > 85?%) and
    b. ions of pore solution + deicing salts.

- Cement paste damage is due to ice growth inside the capillary pores at high degree of water saturation.

  The interface between ice and C-S-H is a thin (nanometers thick) concentrated solution (ions excluded from the freezing water crystals increase the ionic strength of the remaining pore solution).

- In this nanometers-thick liquid layer, ionic pressure develops. It depends on ionic type, concentration, etc.

- Ionic pressure (due to ion confinement) damages C-S-H only if the temperature is cold enough (below -7°C) and the resulting pressure (around a few tens of MPa) exceeds C-S-H strength; otherwise ice melts.

- There is also ionic movement that may be leading to the build-up of this disjoining pressure.

- The phase diagram of bulk water can be used (as water in capillary C-S-H pores is initially under little or no confinement effect) to transform this disjoining pressure into the temperature at which FT damage is likely to occur.

We seek to test this theory portrayed in Figures 21a and 21b and understand the impact of salts on freezing temperature, ice formation, and damage.

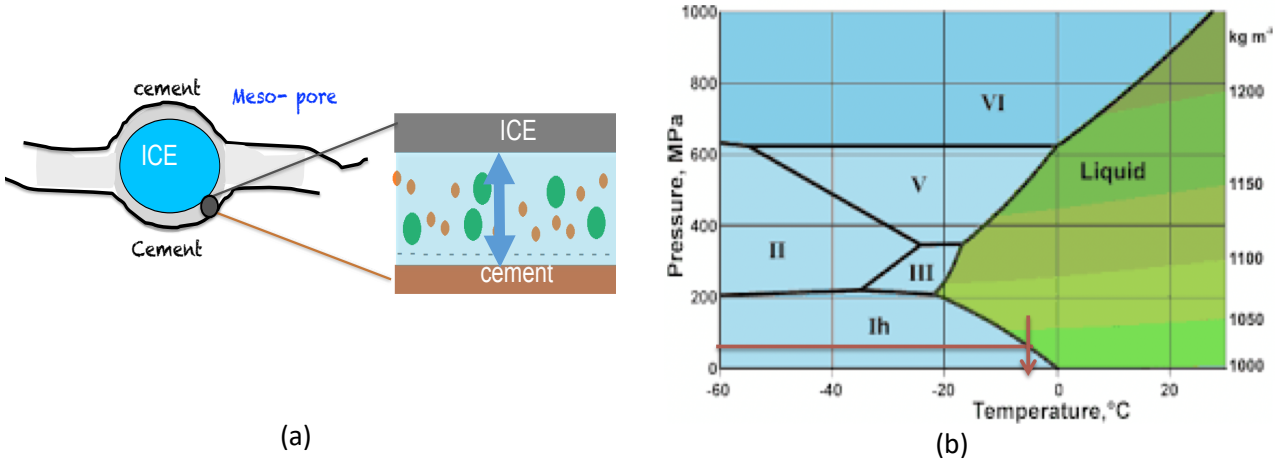

Figure 21: (a) illustration of the osmotic pressure in the interfacial nanometers-thick electrolyte layer between C-S-H and ice, (b) the use of the solidus line in bulk water to transform the osmotic pressure into the temperature at which F – T damage occurs

4.2 Experimental and modeling approach

A multiscale approach for experiments and modeling has been adopted for FT, aiming to link the chemistry (type and concentration of deicing salts) to the altering of the microstructure (pore size distribution, specific surface area) and the impact on the mechanics (crack formation and propagation). Experiments have focused on determining the amount of ice formation and the volume expansion during freezing cycles. Moreover the impact of the deicing solution chemistry on the freezing temperature has been investigated. The modeling approach used here complimented the experiments providing a framework to connect the type and concentration of deicing salts to the change of the microstructure and the formation of cracks.

4.3 Experimental investigation of FT mechanisms

4.3.1 Amount of ice formation

It is important to determine the volume of water that can freeze in a cementitious paste at typical freezing temperatures (i.e., to -13 °C). The freezable water defined here includes water in the air voids, chemical shrinkage voids and capillary pores while the water in gel pores remains unfrozen due to the high capillary pressure caused by the small size of these nano-pores [10, 27, 28]. In order to determine freezable water, cubic-shaped cement paste samples (22 ± 0.5 mg) were obtained from a mature (>91 day) dry specimen (containing no evaporable water, water-to-cement ratio, w/c = 0.35). After 48 hours of saturation in lime water, the samples were preconditioned at different degrees of saturation (DOS) ranging from 24% to 100%. Samples were then immediately placed in hermetically sealed stainless steel containers. Then, the amount of ice formed was quantified using a low temperature differential scanning calorimetry (LT-DSC Q20). The temperature cycle used during the LT-DSC test is shown in Figure 22.

As shown in Figure 23a, 60% of the water freezes at -70°C when the sample is fully saturated (full saturation occurs at room temperature 23C under vacuum); the percentage of freezable water decrease

with DOS and is zero at about 35% DOS [29]. It should be noted that theoretical calculations based on Powers model show 47% of freezable water in a fully saturated paste with a water-to-cement ratio of 0.35, and absence of freezable water at 35% DOS (assuming that 25% of the gel water and all the capillary water is the freezable water). These values are slightly different from those obtained experimentally in part because during theoretical calculations, it is assumed that the mixture has 0% entrapped air, which is not the case for real pastes. In addition, the temperature of the experiments drops to -70°C where some of the water in the gel pores can freeze (based on Kelvins equation and the Gibbs Thomson Equation). Additional testing is underway for various cement paste mixtures. In parallel, in order to prove experimentally that around 35% DOS, only gel pores are filled with water, desorption testing has been performed on the same cement paste sample mixture using Dynamic Vapor Sorption (DVS Q5000) according to the procedure detailed in [30]. The results obtained are shown in Figure 23b. It can be seen that 33% DOS is the limit below which only gel pores are filled with water (i.e., a pore size of 5 nm). This observation is consistent with studies from Powers [31, 32] stating that the limit between non-freezable and freezable pore solution is 5nm.

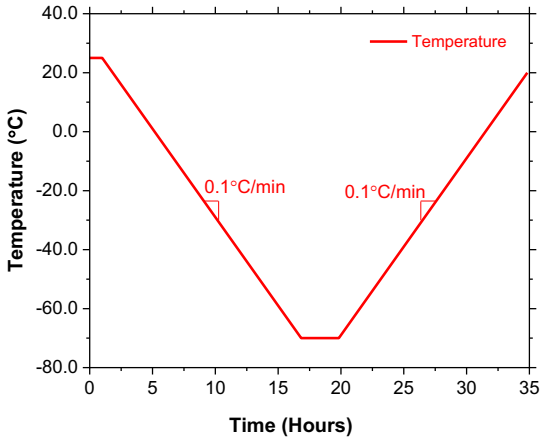

Figure 22: Temperature cycle during the LT-DSC test

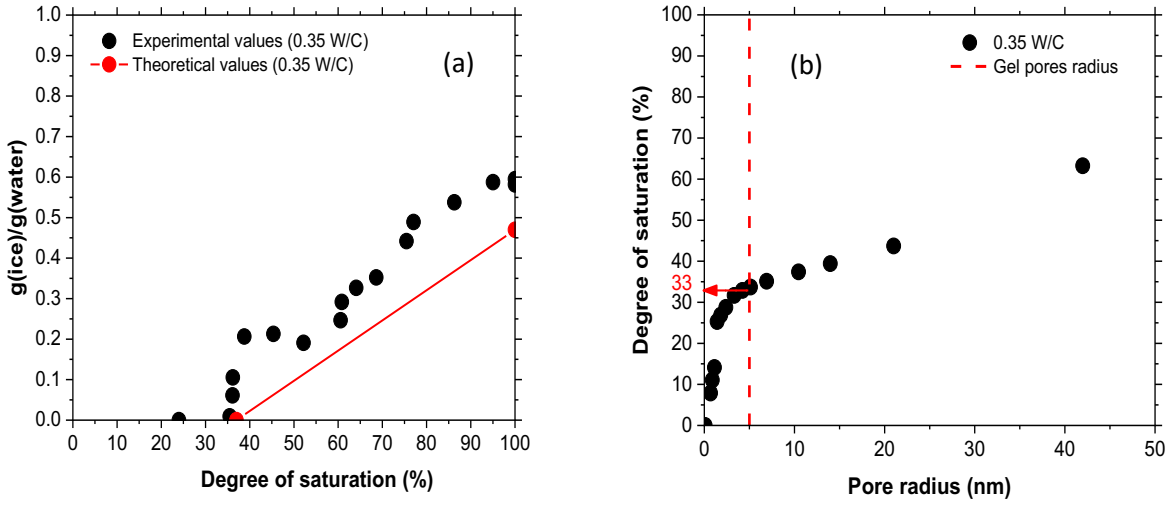

Figure 23: (a) the amount of ice with respect to the degree of saturation, (b) Degree of saturation with respect to the pore radius

4.3.2 Length change measurements during freezing

The impact of the degree of saturation on freezing and thawing cycles was also investigated by measuring the length change of cement paste samples during freezing and thawing cycles using a thermal-mechanical analyzer (TMA Q400). As shown in Figure 24a, cement paste samples with high degree of saturation show expansion and damage during ice formation. The development of damage also results in residual strain after freezing and thawing. For samples below the critical degree of saturation, expansion and damage are not observed (see Figure 24b) [12, 31, 33, 34].

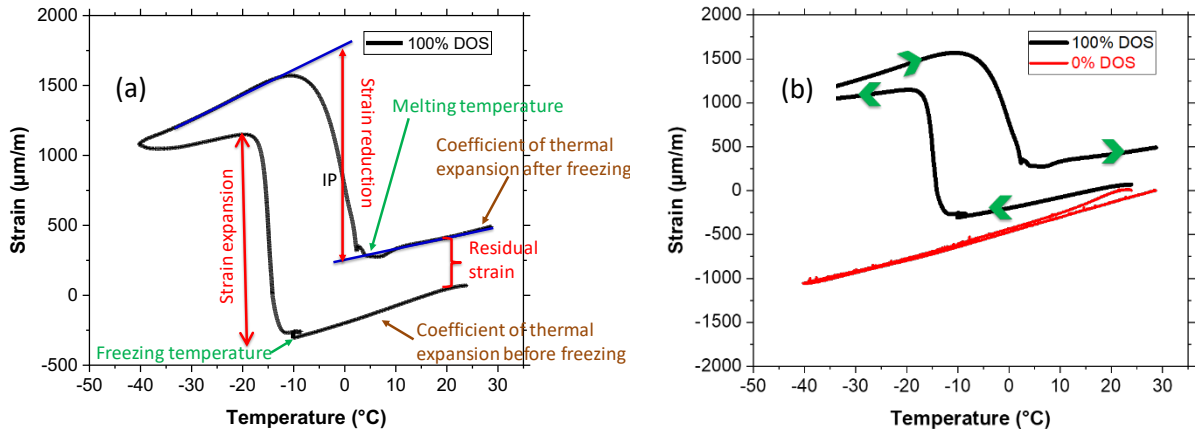

Figure 24: (a) Strain change with respect to temperature: physical meaning of the strain change signal, (b) Impact of DOS on the strain change

4.3.3 Impact of the solution in contact with cement paste on the freezing temperature

In freezing environments, deicing salts are applied on the surface of concrete pavements. Diffusion of salts inside the cementitious matrix changes the freezing temperature of the pore solution. That said it should be noted that the diffusion of ionic species (or their absorption) can occur on length scales of days to years for full depth concrete. Changes in the freezing temperature with different salt solutions can be determined using LT-DSC. LT-DSC was used to measure the heat flow in the hydrated cement paste (w/c=0.36, 91 days old) saturated with different solutions (lime water, 5 % wt. NaCl solution, 10 % wt. NaCl solution, 5 % wt. KCl solution and 10 % wt. KCl solution). The samples were then exposed to the temperature cycle shown in Figure 25. The data analyses were performed on the heating cycle because it is more accurate due to the absence of the undercooling phenomenon [35-37]. According to Figure 26a, the eutectic temperature of aqueous sodium chloride solution in this cement paste is -22.6 °C which is close to the value from the phase diagram of aqueous sodium chloride (-21.1 °C). At a constant eutectic temperature, frozen eutectic transforms from solid to liquid. In the same figure, the ice melting temperature decreases linearly from -0.81 °C to -4.70 °C to -9.03 °C as the concentration of the solution increases from 0% to 5 to 10% NaCl. These experimental results are consistent with literature [11] describing these phenomena by numerical simulation. Figure 26b shows the same information as Figure 26a for potassium chloride solution. The eutectic temperature of aqueous potassium chloride is shown to be equal to -12 °C close to what is reported in literature (-10.7 °C) [38]. Similarly, the ice melting temperature decreases with the increase in the salt solution Figure 27. For both solutions (sodium chloride and potassium chloride), the exact quantification of the enthalpy was not possible due to overlap between ice and eutectic melting as shown in the both Figures 26a and 26b.

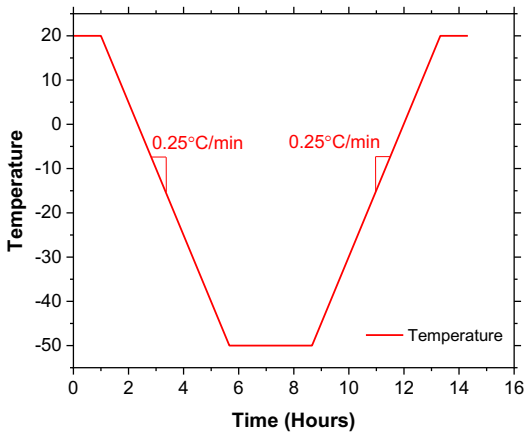

Figure 25: Temperature cycle during the LT-DSC test

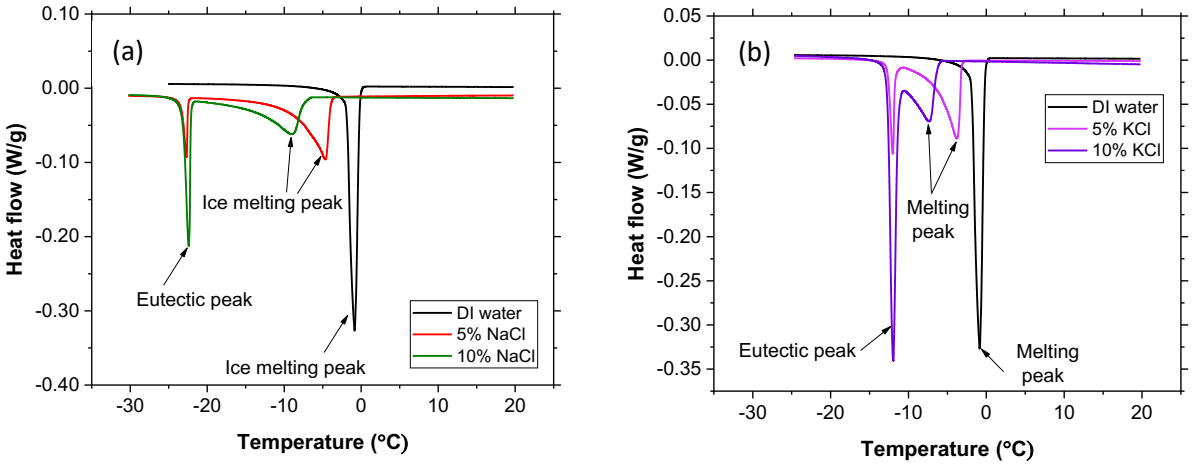

Figure 26: (a) Melting temperatures of ice in pastes saturated with increasing amounts of NaCl, (b) with increasing amounts of KCl

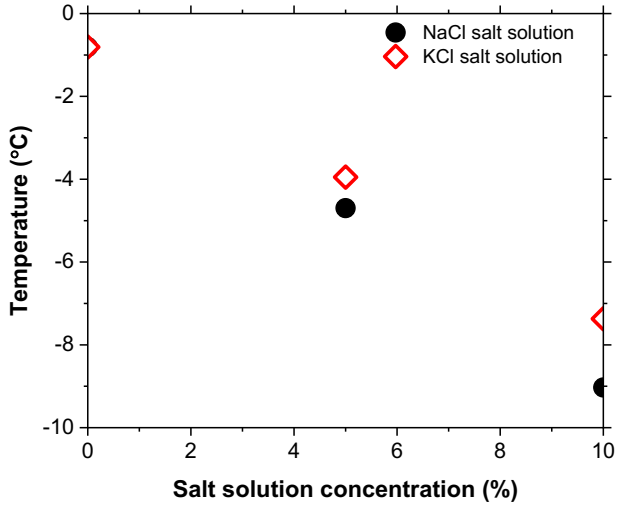

Figure 27: Ice melting temperature with respect to salt solution type and salt solution concentration.

4.3.4 X-ray CT scan Tomography experiments

The MIT team partnered with the Civil Engineering Department of the University of Hannover together with the CEREGE laboratory (CNRS – AMU). Our German colleagues are equipped with an experimental device that allows for a cement paste sample to be loaded with water at 100% saturation (pumping to primary vacuum above the sample partly immersed in water for 5 days) and perform six FT cycles in 24 h from +4°C to -20°C. Our French colleagues in Marseille then performed X-ray CT-scan (view field 80 mm^3, resolution 11 μm) on these samples. Figure 28 shows a 3D picture of a cracked cement sample under the FT conditions described here above. To our knowledge, this is the first 3D image of FT induced micro-cracks in OPC preserved at 100% water saturation during FT cycles.

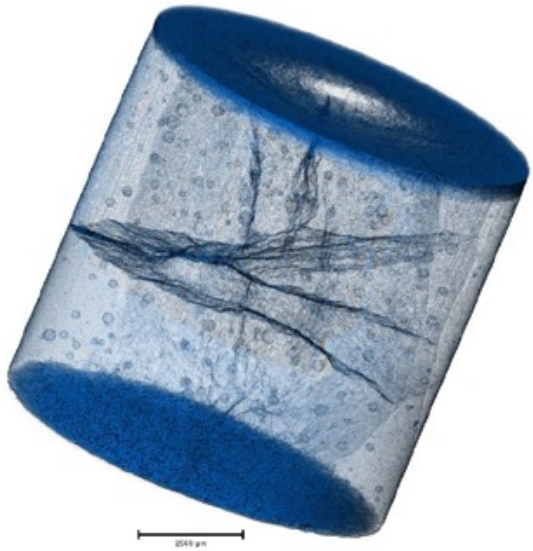

Figure 28: 3D image of an OPC sample with F – T induced micro-cracks, the bar indicates a 2.5 mm scale

4.4 Modeling investigation of FT mechanisms

The modeling effort is based on a computational framework that links chemistry and mechanics. The steps in the modeling effort to understand FT mechanisms are detailed in this section.

4.4.1 Potential of mean force (PMF) for several ion species and concentrations

To study the effect of ions when freezing for an isolated pore, we simulate the pressure of ions confined between an ice surface and the surface of pore in cement paste, as a function of the separation distance. This is motivated by the fact that when freezing occurs, there is a lubricating layer of liquid remaining between the ice and the pore surface, due to thermodynamic effects. When this layer is very thin and pore openings are constricted, the concentrated solution will cause a high pressure build-up, as shown in Figure 29. The pressure vs. separation distance curves can be integrated to derive a potential of mean force (PMF) between ice and C-S-H surfaces.

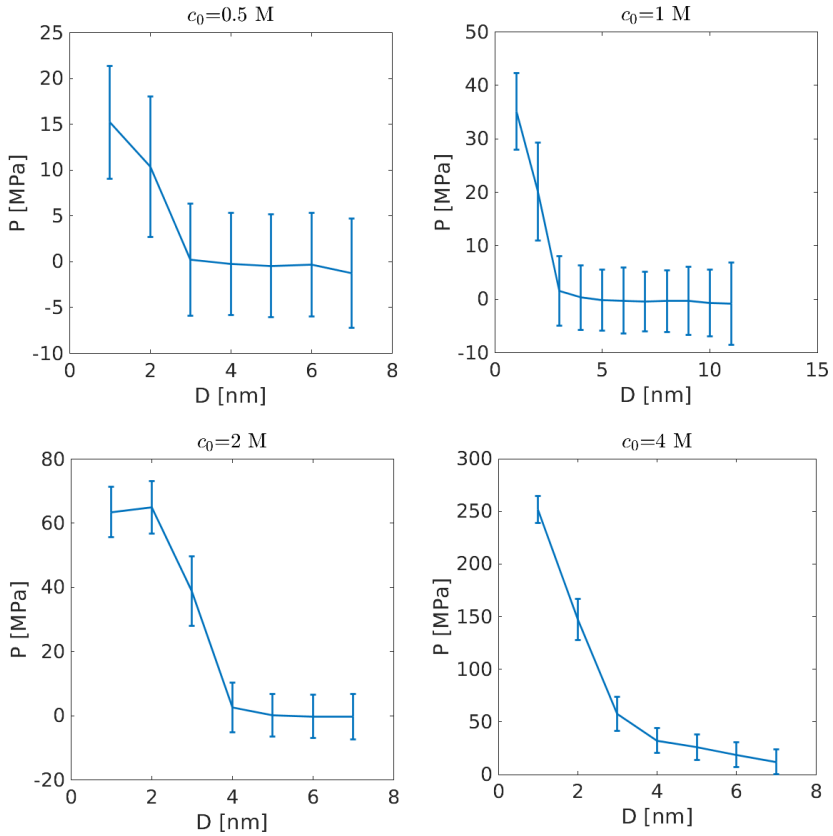

Figure 29: Pressure in the confined nanometers-thick electrolyte layer at the C-S-H – ice interface, with monovalent counter-ions and c_0 showing the concentration of 1:1 salt. Surface charge density of cement nano-particles is assumed -3 e/nm^2. As salt concentration increases, the pressure increases significantly. This is relevant due to solution trapping mechanisms that are described in Section 4.6.5.

Typically, for a 1-nm thick layer, the ionic disjoining pressure increases from 15 to 250 MPa as the ion concentration increases from 0.5 to 4 M. These values largely exceed the tensile strength of hardened paste (10 – 20 MPa). We can then use this knowledge to study the mesoscale results of ice-C-S-H interactions, as shown in the following section.

4.4.2 Effect of different PMFs on mesoscale structure and mechanics

For investigations of the mesoscale structure of cement hydrates, coarse-grained modeling was employed based on nano-sized grains/colloids interacting with effective potentials. The starting point is a mesoscale C-S-H structure spanning a cube of length 390 nm [39, 40]. The C-S-H particles interact with a generalized Lennard-Jones potential:

$$V(r) = 4\,\epsilon\left[\left(\frac{\sigma}{r}\right)^{2\gamma} - \left(\frac{\sigma}{r}\right)^{\gamma}\right] \qquad (4)$$

where σ is the particle diameter, ε the energy and the exponent γ is set to 12. The ice is modeled as a nano-granular material similar to C-S-H but with 12-6 Leonard-Jones interaction between the ice nano-grains (γ=6 in Equation 4). This models the mechanical properties of ice at temperatures equal or lower than -8°C, which is the temperature below which freezing damage is observed. The ice crystal grows via

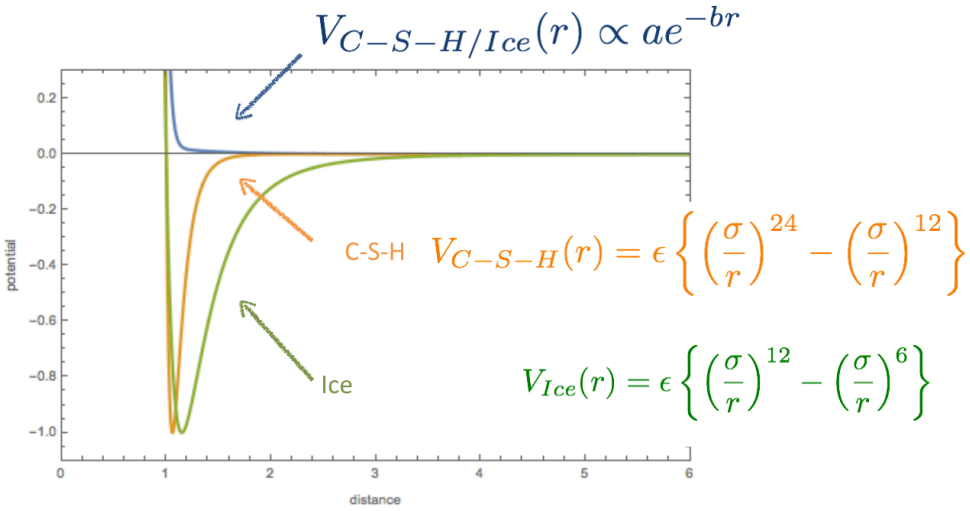

Figure 30: PMF's between different nano-grains describing C-S-H/C-S-H, ice/ice and ice/C-S-H interactions

precipitation simulated by Grand Canonical Monte Carlo (GCMC) model. For this, an open system in the *μVT* statistical ensemble is assumed, where μ is the chemical potential, V the volume of the simulation box and T the temperature. Structural relaxation with molecular dynamics (MD) follows after a GCMC cycle of ice precipitation, similar to Ref. [41]. The MD relaxation was performed in the NPT ensemble with pressure P=0. The water and ions are not explicitly included in the mesoscale simulations. However, the ionic pressure build-up due to the confinement of the ions between C-S-H and ice is included in the calculation of the PMF. The PMF between ice crystal and a C-S-H slab (computed as described in the previous section) provides the effective interaction between the C-S-H and ice nano-grains. Figure 29 summarizes all interactions. Through the simulations we observe three stages of structural changes. Initially, the ice fills the pores resulting in local compaction of the C-S-H solid matrix. The volume of the simulation box increases once the ice has percolated through the 3D pore network of C-S-H. This signals the creation of micro cracks that fracture the micron-scale sample. Figure 31 shows a crack fracturing the sample due to ice precipitation.

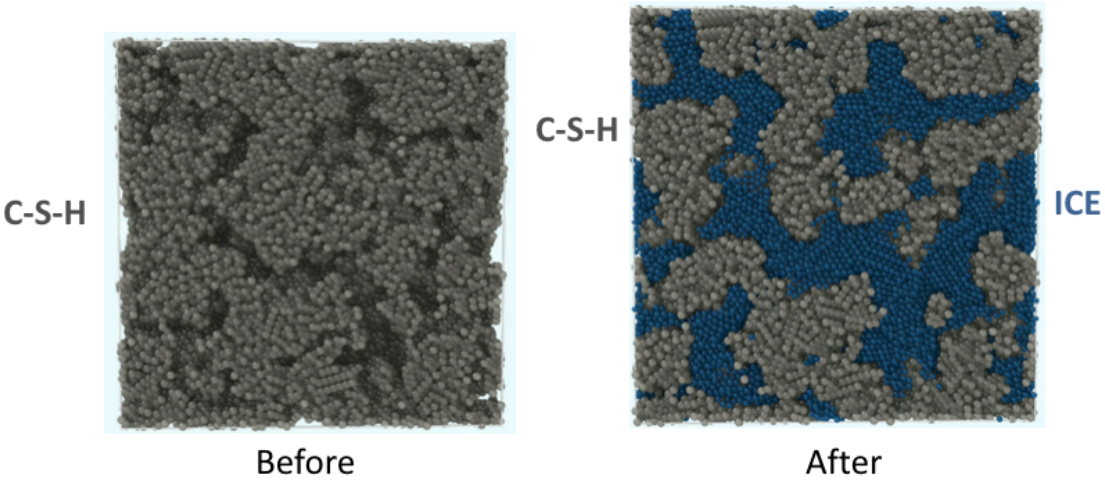

Figure 31: Left snapshot shows the solid matrix composed of C-S-H particles before freezing. Right snapshot shows the same sample after freezing. Blue particles stand for the ice. The overall volume of the sample has increased and cracks 3D-percolate the sample.

4.4.3 Locate capillary water for different DS in the mesoscale model (lattice DFT)

We developed a numerical framework to calculate the distribution of water inside the pores in cement paste (see [42, 43] and Figure 32). Locating this confined water is necessary to fully understand freeze-thaw mechanisms, since there is experimental evidence that the degree of saturation needs to reach a critical value for FT damage. Based on previous meso-scale modeling of cement paste texture, the spatial distribution of water can be identified at any relative humidity, and the effect of these water menisci can be estimated.. According to our investigations, they actually can affect the structure on the nano-scale and cause irreversible deformations, when the cement/concrete undergoes drying. Although these deformations are localized and not percolating to directly cause damage, they later initiate weak spots for damage when mechanical loading is applied [42, 43, 55].

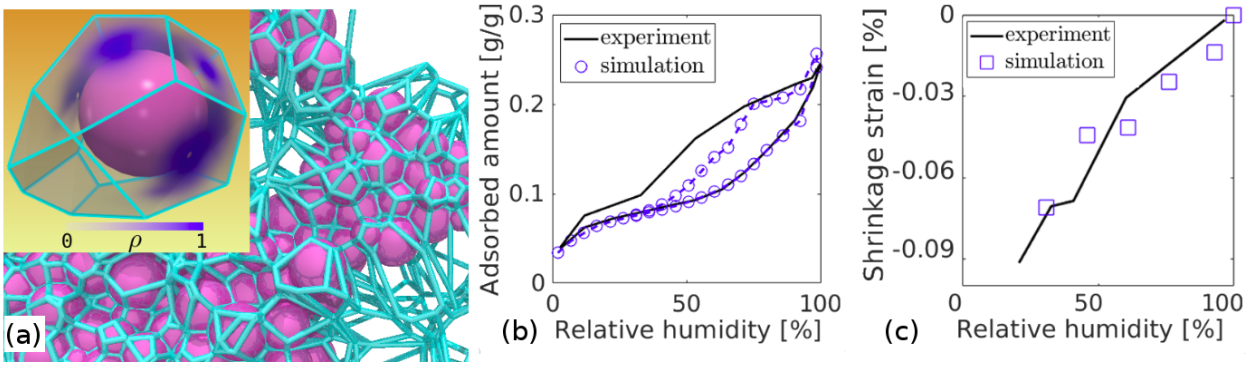

Figure 32: (a) Schematics of the tessellation scheme around C-S-H nano-grains with adsorbed water. Pink spheres represent C-S-H particles. Green columns show the edges of Voronoi tessellation. Inset shows the liquid density distribution around a C-S-H particle. (b) Simulated water adsorption/desorption isotherm on cement paste model of Ref. [39]*, compared to experiment data from Ref* [45] *(c) simulated first drying shrinkage curve of cement paste, compared with experiment data from Ref.* [46].

4.4.4 Compare pore size distribution, chord length distribution and specific surface area from mesoscale simulation with experiments

Initially the structural changes in the C-S-H solid matrix are characterized using pore size distributions (PSD). PSD is established as described in Ref [44]. Figure 33 shows the PSD of the C-S-H solid matrix without ice crystals. The red line represents the initial PSD, the black line represents the PSD when the ice percolates the sample, and the green line represents the final state. At the final state, the overall porosity of the sample has increased due to the volume expansion. Therefore, the volume of the larger C-S-H pores (25-40 nm) increase. This is also confirmed from the chord length distributions of the pores in Figure 34. The chord length distribution is computed as in Ref. [39].

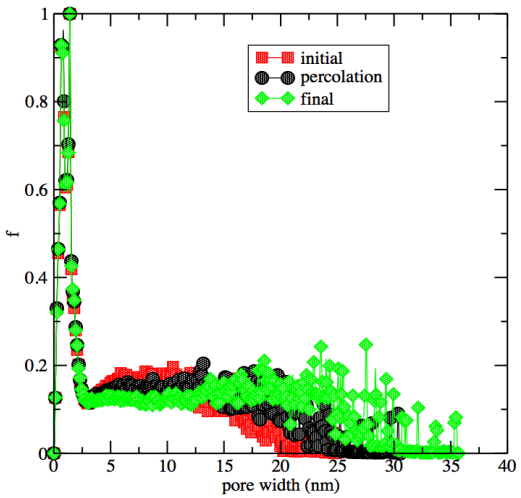

Figure 33: Pore size distribution at different stages of the ice precipitation.

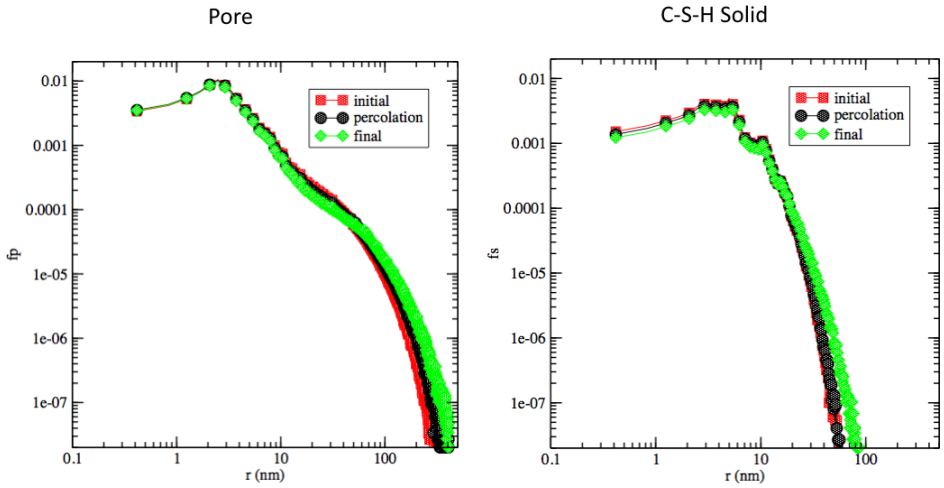

Figure 34: Chord length distributions for the C-S-H solid matrix. Left (Right) plot show the distribution of chords in the pore (solid).

4.4.5 Mechanism of pressure generation: nano-fluidic salt trapping

A theory is proposed for freezing phenomena in charged porous media that explains the various experimental aspects observed in FT of cement paste. This theory suggests that the connectivity and wide distribution of pore sizes, as well as ionic concentration of the pore solution are the key to FT damage. The theory predicts large pressure built up only if large pores are filled with liquid and freeze first. When this occurs, a very thin lubricant layer of solution remains between the ice formed and the pore wall (see Figure 35a). These liquid pathways provide extremely low accessibility of the salt ions inside smaller pores to the outside, hence effectively the salt ions in those small pores are trapped (see [47-49]). As the temperature continues to drop, ice crystals nucleate in the small pores causing a pressure increase that is transmitted to the pore wall. Ion concentration will increase at the same time since water molecules can escape through the aforementioned liquid pathways faster because they are neutral (see Figure 35b). If temperature continues to drop, eventually salt ions reach a saturated concentration and precipitate to form salt crystals, as a result of pressure. This crystallization is not the cause of pressure.

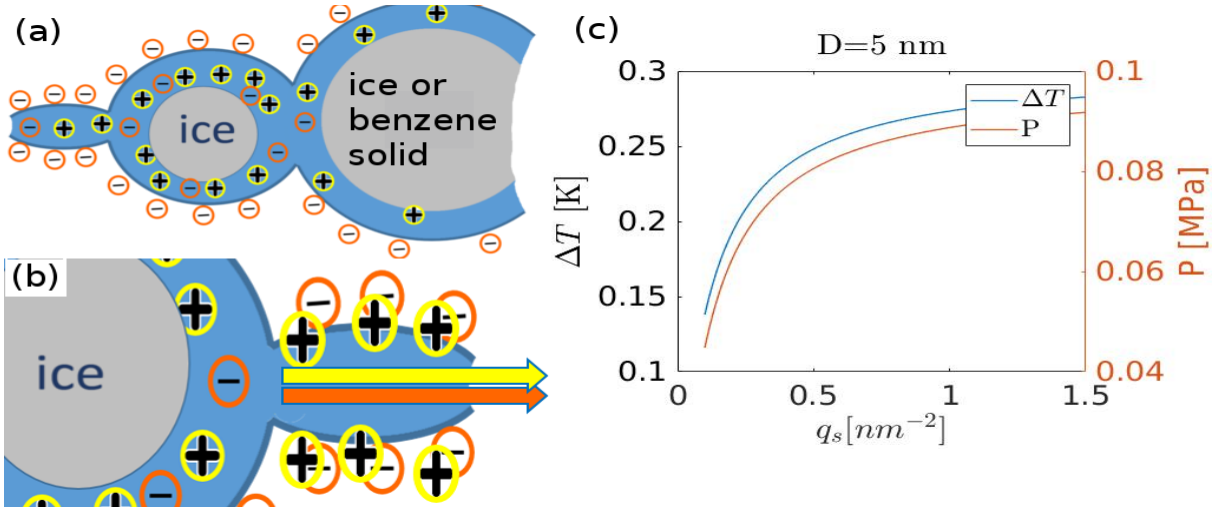

Figure 35: (a) Above a critical degree of saturation, the large pores are filled by water and freeze first. Water molecules can escape but salt ions inside capillary pores are trapped by charged nano-pores and cause pressure. (b) nano-fluidic channel opens for ions when concentration is too high. (c) When large pore is empty and ions are free to leak, no large pressure is expected in the capillary pores.

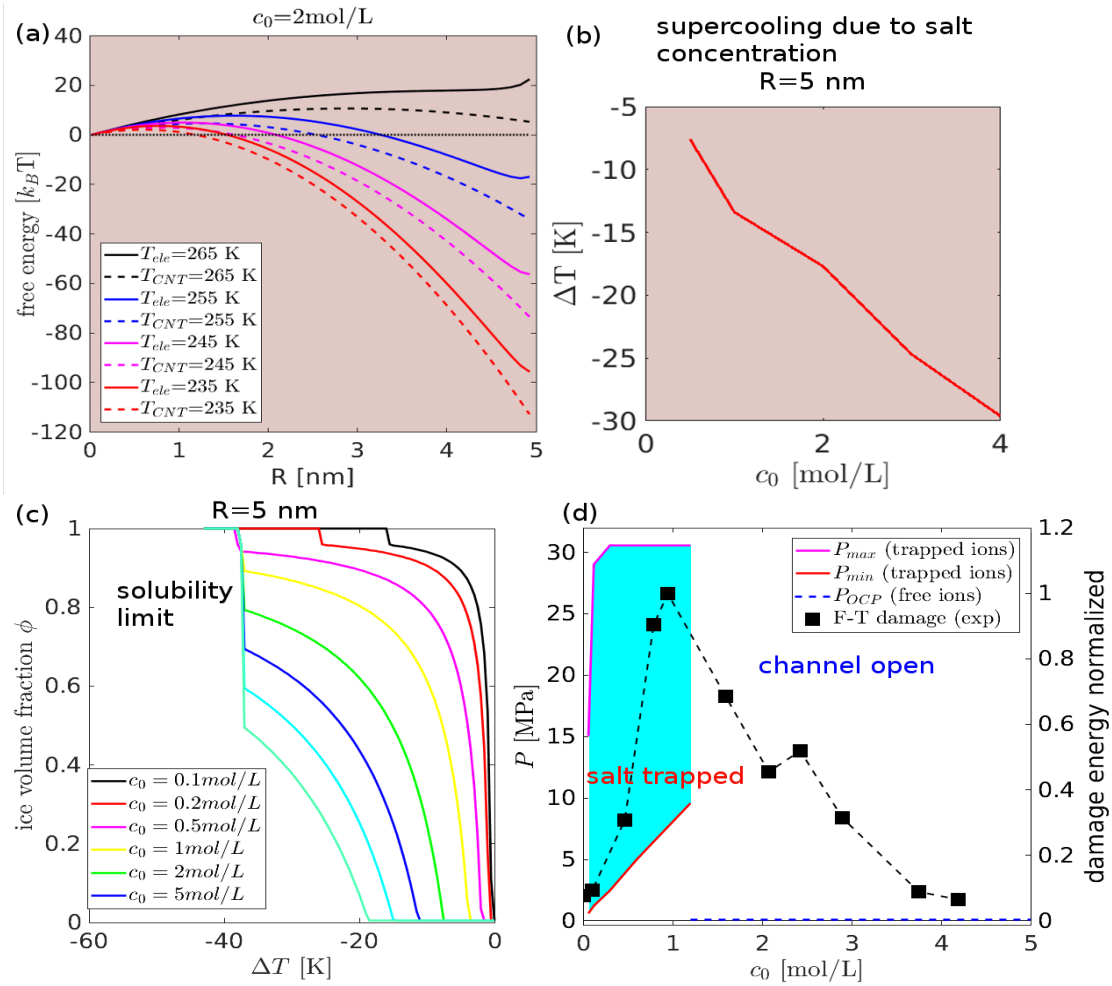

Figure 36: (a) free energy functional of ice formation in a 5 nm pore. Solid lines calculated from classical nucleation theory, dashed ones includes contribution from salts. (b) additional supercooling due to salt concentration. (c) ice volume fraction in the pore, as a function of salt concentration and temperature. All curves terminate at the solubility limit of the solute, where salt crystallization happens as a result. (d) Min and Max pressure during ice formation. Above a threshold concentration the nano-fluidic channels open and salt ions are released from the freezing pore--- pressure decreases. Qualitative same trend as the experiment data from ref. [50].

This theory is supported by several key experimental observations:

- Critical degree of saturation for FT: if saturation is less than a critical level, the large pores are empty and will not freeze. When water in the small pores freeze, solution exits through these large empty pores, leaving behind only the counter-ions that neutralize the charge of the pore walls. In this case very minimal pressures of 0.1 MPa is predicted and causes no damage (see Figure 36c).

- Damage as a non-monotonic function of salt concentration: As salt concentration increases, experimentalists first see signals of increasing damage, until a critical concentration is exceeded, following which damage decreases. In this theory (see Figure 36d), the trapping mechanism is due to the surface charge of the pore walls. When salt concentration increases, ionic concentration increases in the small pores and larger pressure is expected. However, when concentration is too high, charge regulation will neutralize the pore walls, and the trap is essentially released. As a result, the trapped ions start to escape and pressure will decrease.

4.5 Synthesis: what causes the pressure in FT-affected concrete?

Combining the knowledge gained from experiments run at MIT, OSU, Hannover and CNRS-AMU together with multiscale simulation results carried out at MIT, we are now in a position to clarify several key points and propose a realistic scenario for FT in accordance with all experimental facts. First, for FT damage to occur, two key ingredients must be present: (i) a high saturation level, and (ii) the presence of high ionic concentration in the C-S-H/ice interface in capillary pores. Here are key findings from the work coordinated by the CSHub and CNRS in collaboration with Hannover U. and AMU.

- FT damage to concrete requires a high level of saturation of the cement paste porosity (>80%). As the temperature decreases, ice crystals in capillary pores start forming and expelling ions in the nanometers-thick solution layer remaining in between the charged surface of C-S-H and the neutral (or quasi-neutral) surface of ice.

- Simulations in a primitive model using a one-plasma component approach of statistical physics reveal that the interactions between the ionic species (especially alkali) confined in a nanometer-thick solution layer in between the charged surface of C-S-H and the neutral (or quasi-neutral) surface of the ice crystals creates an osmotic disjoining pressure.

- A key finding of this work was to demonstrate that this disjoining pressure at the C-S-H/ice interface caused by this liquid layer eventually exceeds the C-S-H matrix strength and causes damage. This is clearly a new result that sheds new light on the FT mechanism based on a realistic description of physical chemistry interactions. These simulations also demonstrate that alkali ions in the wetting layer induce a disjoining pressure larger than that with alkaline earth species. This disjoining pressure

increases non-linearly as the ion concentration increases in the interfacial layer: at constant layer thickness, the larger the concentration, the larger the disjoining pressure and thereby damage occurs at a lower temperature. Figure 37 compares experiment and simulation results and shows a good agreement between the two sets of results, which is in itself remarkable given the simplicity of the primitive model description for the simulation of the interfacial electrolyte layer leading to a constant overestimate of the damage temperature by +2°C at all salt concentrations.

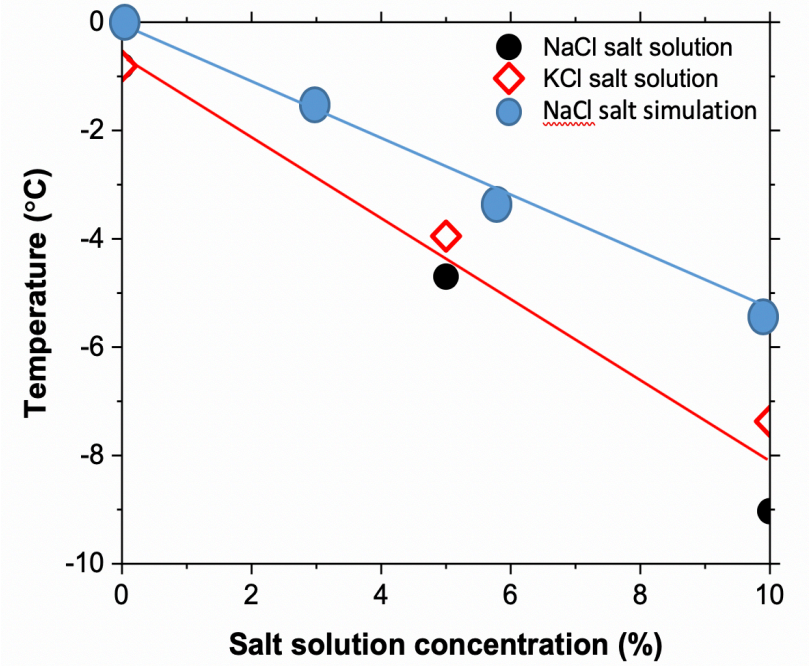

Figure 37: Ice melting temperature with respect to salt solution type and salt solution concentration. The line illustrates the decrease of the temperature at which F – T damage occurs as a function of the salt concentration (red) experiments, (blue) primitive model simulation

- Coarse grained mesoscale simulations were also in agreement with tomography experiments that repulsive disjoining interaction between C-S-H and ice crystals leads to the failure of the C-S-H paste at the micron scale inducing micro-cracks. Furthermore, these mesoscale simulations also revealed that these cracks actually form the capillary pores that can be seen as an initial weak point of the cement hydrate matrix. This indicates that durability of a cement paste is impacted by the initial water-to-binder ratio; a low w/b ration improves the durability of the paste.

In conclusion, by combining mechanical and characterization experiments together with atomistic and mesoscale simulations, we conclude that that FT damage is not the result of direct contact between ice crystals and the C-S-H matrix, but appears to be the consequence of a disjoining pressure due to ionic concentration of a nanometers-thick solution layer at the C-S-H/ice interface in the capillary pore network. The simulated effects of the type of ions and their concentration in the model are validated by the experimental data.

4.6 Mitigation: what can we do to avoid FT damage?

Having identified the key role of the liquid nanometers-thick layer at the C-S-H/ice interface in creating a disjoining pressure large enough to exceed C-S-H matrix strength, a mitigation strategy is proposed. First

this pressure finds its origin in the existence of ions that diffuse in a interfacial water layer at the capillary pore surface. Eliminating this water will prevent any ionic movement and hence suppress the ionic disjoining pressure between C-S-H and ice. In other words, making C-S-H pores hydrophobic is therefore a good strategy to mitigate FT.

We propose to dope cement hydrate paste with black or porous carbon. A carbon / (binder + water) ratio around 5 % produces a black cement paste that has the property of conducting electrons like a piece of metal because of the percolative network of carbon black nanoparticles (characteristic size: 200 nm) confined to the large capillary pores of the cement paste. This hydrophobic substance in the cement paste will naturally reduce the amount of water in the capillary pores. Besides the e-conduction property, carbon-doped cement paste also exhibits an interesting Joule effect: the polarization of a 2 cm^3 cylinder of "black cement" with a few volts allows an increase of the external sample surface up to 100°C with respect to the ambient room temperature. This effect leads to water vaporization and hence, reduces the water content in the cement paste capillary pores, which reduces / removes any FT related ionic disjoining pressure. In addition, we found that adding a hydrophobic substance such carbon-black nanoparticles that dock into C-S-H large capillary pores readily improves the resistance to FT even in zero electrical polarization conditions. We performed (in collaboration with Hannover University, CNRS and Aix-Marseille University) CT scan-type X-ray tomography experiments on carbon-doped cement (23 % carbon weight percent with respect to the total water + carbon + cement mix). After six FT (+4°C → -20°C → +4°C) cycles at **100 % water saturation** the carbon loaded sample did not exhibit any microcrack pattern as opposed to the pure cement paste (see Figure 38).

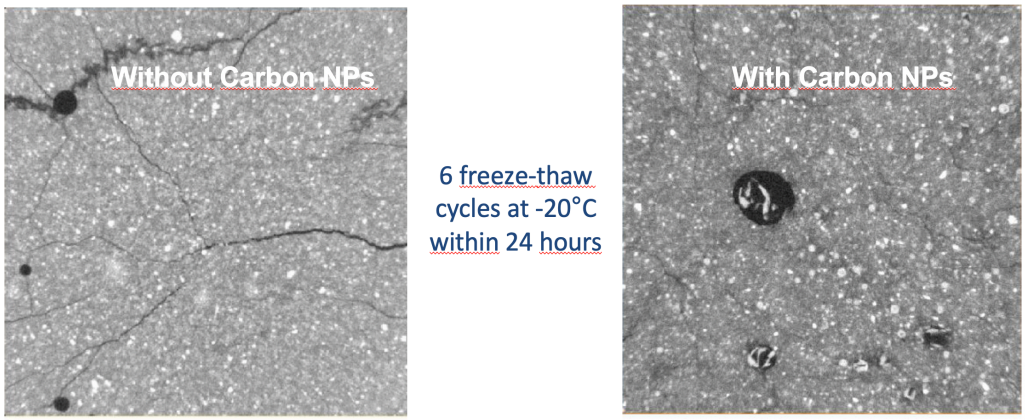

Figure 38: SEM pictures of pure and carbon-loaded cement pastes after FT cycles.

References:

[1] Weiss, J., C. Qiao, and P. Suraneni, Synthesis: Accelerating the implementation of research findings to reduce the potential concrete pavement joint deterioration (submitted in 2018). Joint Transportation Research Program
[2] Mayercsik, N.P., M. Vandamme, and K.E. Kurtis, Assessing the efficiency of entrained air voids for freeze-thaw durability through modeling. Cement and Concrete Research, 2016. 88: p. 43-59.
[3] Felice, R.V., Frost resistance of modern air entrained concrete mixtures. 2012, Oklahoma State U.
[4] Ghantous, R.M., et al., The influence of carbonation on the formation of calcium oxychloride. Cement and Concrete Composites, 2016. 73: p. 185-191.
[5] Powers, T.C. and T.F. Willis, The air requirement of frost resistant concrete. Proceeding of Highway Research Board, 1950. 29: p. 189-211.

[6] Qiao, C., P. Suraneni, and J. Weiss, Damage in cement pastes exposed to NaCl solutions. Construction and Building Materials, 2018. 171: p. 120-127.
[7] Qiao, C., P. Suraneni, and J. Weiss, Flexural strength reduction of cement pastes exposed to CaCl2 solutions. Cement and Concrete Composites, 2018. 86: p. 297-305.
[8] Qiao, C., et al., Damage in cement pastes exposed to MgCl2 solutions. Materials and Structures, 2018
[9] Ghazy, A. and M.T. Bassuoni, Resistance of concrete to different exposures with chloride-based salts. Cement and Concrete Research, 2017. 101: p. 144-158.
[10] Li, W., et al., Water absorption and critical degree of saturation relating to freeze-thaw damage in concrete pavement joints. Journal of Materials in Civil Engineering, 2011. 24(3): p. 299-307.
[11] Esmaeeli, H.S., et al., Numerical simulation of the freeze–thaw behavior of mortar containing deicing salt solution. Materials and structures, 2017. 50(1): p. 96.
[12] Ghantous, R.M., et al., Examining the influence of the Degree of Saturation on Length Change and the amount of ice and Associating Freeze-Thaw Damage with Critical Degree of Saturation In the process of being written 2018.
[13] Fagerlund, G., The international cooperative test of the critical degree of saturation method of assessing the freeze/thaw resistance of concrete. Matériaux et Construction, 1977. 10(4): p. 231-253.
[14] Todak, H.N., Durability assessments of concrete using electrical properties and acoustic emission testing, in School of Civil Engineering. 2015, Purdue University: West Lafayette. p. 143.
[15] Lucero, C.L., Quantifying moisture transport in cementitious materials using neutron radiography, in Civil Engineering. 2015, Purdue University: West Lafayette, IN, USA. p. 130.
[16] Bentz, D.P., et al., Sorptivity-based service life predictions for concrete pavements, in 7th International Conference on Concrete Pavements. 2001, International Society for Concrete Pavements: Orlando, FL. p. 181-193.
[17]Lucero, C.L., et al., Using Neutron Radiography to Quantify Water Transport and the Degree of Saturation in Entrained Air Cement Based Mortar. Physics Procedia, 2015. 69(Supplement C): p. 542-550.
[18] Powers, T.C. and T.L. Brownyard, Studies of the physical properties of hardened portland cement paste. Bulletin 22. 1948, Chicago: Research Laboratories of the Portland Cement Association.
[19] Todak, H., C. Lucero, and J. Weiss, Why is the air there? Thinking about freeze-thaw in terms of saturation. Concrete inFocus, 2015: p. 3-7.
[20] Azad, V.J., et al., Interpreting the pore structure of hydrating cement phases through a synergistic use of the Powers-Brownyard model, hydration kinetics, and thermodynamic calculations. Advances in Civil Engineering Materials, 2017. 6(1): p. 1-16.
[21] Glosser, D., et al., An integrated thermodynamic, kinetics, and Powers-Brownyard model for OPC-SCM (submitted in 2018). ACI Materials Journal
[22] Jensen, O.M., et al., Chloride ingress in cement paste and mortar. Cement and Concrete Research, 1999. 29(9): p. 1497-1504.
[23] Jensen, O.M. and P.F. Hansen, Water-entrained cement-based materials: I. Principles and theoretical background. Cement and concrete research, 2001. 31(4): p. 647-654.
[24] Igarashi, S.-i., M. Kawamura, and A. Watanabe, Analysis of cement pastes and mortars by a combination of backscatter-based SEM image analysis and calculations based on the Powers model. Cement and Concrete Composites, 2004. 26(8): p. 977-985.
[25] Li, W., et al., Using neutron radiography to assess water absorption in air entrained mortar. Construction and Building Materials, 2016. 110: p. 98-105.
[26] Mindess, S. and J.F. Young, Concrete. 2nd ed. 2002, Englewood Cliffs, NJ: Prentice Hall.
[27] Sun, Z. and G.W. Scherer, Pore size and shape in mortar by thermoporometry. Cement and Concrete Research, 2010. 40(5): p. 740-751.
[28] Sun, Z. and G.W. Scherer, Effect of air voids on salt scaling and internal freezing. Cement and Concrete Research, 2010. 40(2): p. 260-270.

[29] Ghantous, R.M., et al. Experimental and numerical characterization of load-induced damage in reinforced concrete members. Berkeley.
[30] Qiao, C., W. Ni, and J. Weiss, Transport due to Diffusion, Drying, and Wicking in Concrete Containing a Shrinkage-Reducing Admixture. Journal of Materials in Civil Engineering, 2017. 29(9): p. 04017146.
[31] Powers, T.C. and R. Helmuth. Theory of volume changes in hardened portland-cement paste during freezing. in Materials and construction. 1953.
[32] Powers, T.C. A working hypothesis for further studies of frost resistance of concrete. in Journal Proceedings. 1945.
[33] Bazant, Z.P., et al., Mathematical Model for Freeze-Thaw Durability of Concrete. Journal of the American Ceramic society, 1988. 71(9): p. 776-783.
[34] Trofimov, B.Y., L.Y. Kramar, and K. Schuldyakov. On Deterioration Mechanism of Concrete Exposed to Freeze-Thaw Cycles. in IOP Conference Series: Materials Science and Engineering. 2017. IOP Publishing.
[35] Askeland, D.R., P.P. Fulay, and W.J. Wright, The science and engineering of materials. 2011, Stamford, CT: Cengage Learning.
[36] Debenedetti, P.G., Supercooled and glassy water. Journal of Physics: Condensed Matter, 2003. 15(45): p. R1669.
[37] Wilding, C., The performance of cement based systems. Cement and concrete research, 1992. 22(2-3): p. 299-310.
[38] Barnes, W. and O. Maass, Freezing Points and Heat Capacities of Aqueous Solutions of Potassium Chloride. Canadian Journal of Research, 1930. 2(3): p. 218-229.
[39] Ioannidou, K.; Krakowiak, K. J.; Bauchy, M.; Hoover, C. G.; Masoero, E.; Yip, S.; Ulm, F.-J.; Levitz, P.; Pellenq, R. J.-M.; Del Gado, E. Mesoscale Texture of Cement Hydrates. Proc. Natl. Acad. Sci. 2016, 113 (8), 2029–2034
[40] Ioannidou, K.; Gado, E. Del; Ulm, F.-J.; Pellenq, R. J.-M. Inhomogeneity in Cement Hydrates: Linking Local Packing to Local Pressure. J. Nanomechanics Micromechanics 2017, 7 (2), 4017003
[41] Ioannidou, K.; Pellenq, R. J.-M.; Del Gado, E. Controlling Local Packing and Growth in Calcium-Silicate-Hydrate Gels. Soft Matter 2014, 10, 1121–1133
[42] Zhou, Tingtao, Katerina Ioannidou, Enrico Masoero, Mohammad Mirzadeh, Roland Pellenq, and Martin Bazant. "Capillary stress and structural relaxation in moist granular materials", Langmuir 35, 4397-4402 (2019).ƒ43
[43] Zhou, Tingtao, Ioannidou Katerina, Ulm Franz J., Bazant Martin Z., and Pellenq Roland, J.-M. “Multiscale Poromechanics of wet cement paste”, Proc. Natl. Acad. Sci., 2019, 116 (22), 10652-10657
[44] Bhattacharya, S., and Gubbins, K. E. (2006). “Fast method for computing pore size distributions of model materials.” Langmuir, 22(18), 7726–7731
[45] Baroghel-Bouny, Véronique. "Water vapour sorption experiments on hardened cementitious materials: Part I: Essential tool for analysis of hygral behaviour and its relation to pore structure." Cement and Concrete Research 37, no. 3 (2007): 414-437.
[46] Feldman, Rolf F., and Peter J. Sereda. "A model for hydrated Portland cement paste as deduced from sorption-length change and mechanical properties." Matériaux et Construction 1, no. 6 (1968): 509-520.
[47] Yossifon, Gilad, Yu-Chen Chang, and Hsueh-Chia Chang. "Rectification, gating voltage, and interchannel communication of nanoslot arrays due to asymmetric entrance space charge polarization." Physical review letters 103, no. 15 (2009): 154502.
[48] Biesheuvel, P. M., and M. Z. Bazant. "Analysis of ionic conductance of carbon nanotubes." Physical Review E 94, no. 5 (2016): 050601.
[49] T. Zhou, M. Mirzadeh, R.J.-M. Pellenq, and M. Z. Bazant. “Surviving winter: theory of freezing point depression by salt trapping in charged porous media.” in preparation.

[50] Farnam, Yaghoob, Dale Bentz, Aaron Sakulich, Daniel Flynn, and Jason Weiss. "Measuring freeze and thaw damage in mortars containing deicing salt using a low-temperature longitudinal guarded comparative calorimeter and acoustic emission." Advances in Civil Engineering Materials, 3 (2014), 316
[51] P.J.M. Monteiro and J. Bastacky, ACI Materials Journal, V99 (N2): 190-195, Mar-Apr 2002.
[52] ACI Committee 201 Report, Guide to Durable Concrete, American Concrete Institute (1992).
[53] V. Penttala, “Freezing-Induced Strains and Pressures in Wet Porous Materials and Especially in Concrete Mortars”, Advanced Cement Based Materials, 7(1): 8-19 (1998).
[54] Powers, T.C.: “Freezing Effects in Concrete”, Paper from symposium sessions, held in Atlantic City, New Jersey and Ottawa, Ontario, 1973. Published in “Durability of concrete”, SP-47, American Concrete Institute, Detroit, 1975.

5 Outlook

5.1 Classical methods to avoid FT and Salt damage

As reported in [1, 2], several methods allow for reducing the potential of freeze-thaw damage. These classical methods include ways to reduce the potential for reaching critical saturation by using greater air content and well-dispersed air voids [3], and the use of surface treatments that reduce the rate of fluid absorption [4]. While joint damage may be considered to be due to freeze-thaw damage this damage may more likely be due to the formation of calcium oxychloride resulting from the use of deicing chemicals, it is important to consider methods such as the use of supplementary cementitious material replacement [5-7], the use of deicer salt blends with greater sodium chloride content [8] the use of topical treatments and carbonation [9], and greater air entrainment [10], which reduce the damage associated with calcium oxychloride formation .

5.2 Economic impacts of freeze-thaw damage

A model has been used to predict the onset of freeze thaw damage that is being implemented by FHWA's Performance Related Specifications for Pavement Construction program. More details about this model can be found in [8, 9]. This model takes into account the impact of air void system and volume on the performance of concrete in freeze-thaw environment. Indeed, variability is an important factor in the freeze-thaw performance of concrete including pavement performance. The variation in air content [10] and spacing has been related to the time to reach critical saturation and is currently being implemented in FHWA life-cycle performance models (i.e., RigidPave) [9].

Figure 39a shows the results of Monte Carlo simulations to illustrate the impact of variability on the simulated time to reach critical saturation. This illustrates that for a mixture with 7% air, 10% of the mixtures fail at 20 years despite the average performance (see Figure 39b) predicts nearly double the service life. This indicates that while having sufficient average air specified is key, controlling the variation in the air content in the field is significant in terms of the pavement repair cycles and service life cost.

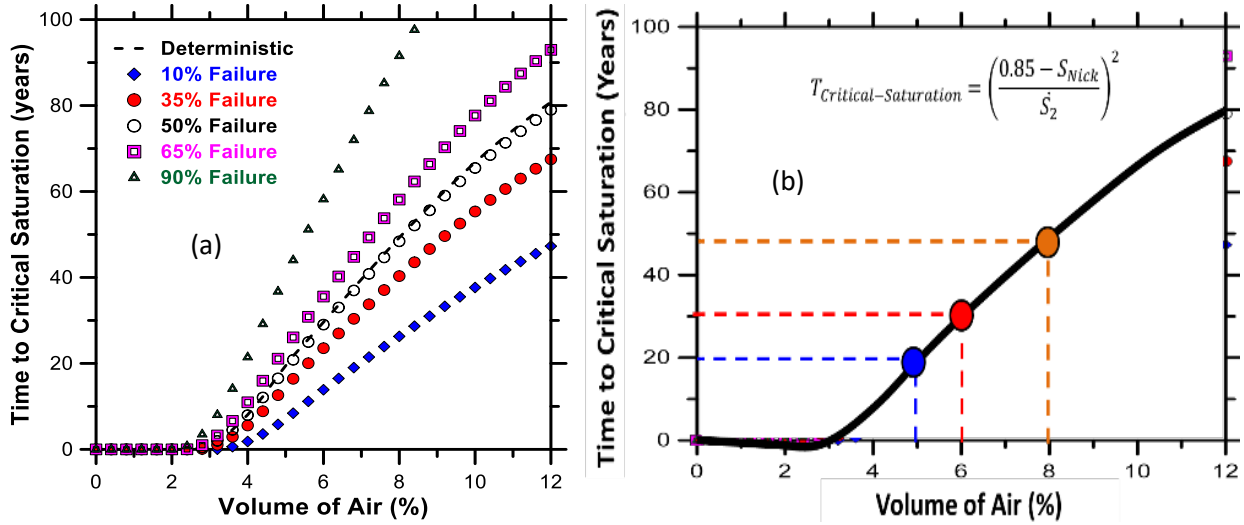

Figure 39: Time to critical saturation for concrete versus air content: (a) Monte Carlo simulation, (b) Model developed based on bucket test results (analyses conducted by OSU)

5.3 A science-grounded engineering solution to mitigate freeze-thaw and ASR

One of the main outputs of this report is the conceptualization of ASR and FT in a unified theoretical framework that is well-grounded in science and has the potential of directly fueling engineering development.

FT: by combining mechanical and characterization experiments together with atomistic and mesoscale simulations, we found that there is NO direct contact between ice crystals and the C-S-H matrix resulting in damage. FT damage in concrete/cement paste appears to be the consequence of a disjoining ionic pressure at the C-S-H/ice interface in the capillary pore network that is able to fracture the C-S-H matrix. The simulated effects of the type of ions and their concentration agree well with experiments (see Figure 37.

ASR: by combining mechanical and characterization experiments together with atomistic and mesoscale simulations, we found that there is NO direct effect of a swelling ASR gel resulting in C-S-H matrix damage. ASR damage is proposed to be the consequence of a Na←→ Ca exchange mechanism between a "pristine" (Ca-poor) alkali gel produced by the reactive aggregates and cement hydration products over time that creates a disjoining ionic pressure at the C-S-H/"old" (Ca-rich) ASR gel interface in the capillary pore network able to fracture the C-S-H matrix. This is a general result for any in-pore-solidification mechanism, as shown in the experimental work of Desarneau et al. [13] demonstrating the role of the nanometer-thick interfacial electrolytic layer in the case of FT damage of monument rocks.

Having identified for both ASR and FT, a potential key role of a nanometers-thick liquid layer at the C-S-H/ASR gel interface or the C-S-H/ice interface in creating a disjoining pressure large enough to exceed C-S-H matrix strength, we propose to dope cement hydrate paste with black or porous carbons. A carbon / (binder + water) ratio around 5% produces a black cement paste that has the property of conducting electrons like metal thanks to the percolative network of carbon black nanoparticles (characteristic size: 200 nm) confined to the large capillary pores of the cement paste. This hydrophobic substance in the cement paste will naturally reduce the amount of water in the capillary pores. Besides the electrical conductivity, carbon-doped cement paste also exhibits an interesting Joule effect: the polarization of a 2 cm3 cylinder of "black cement" with a few volts allows an increase of the external sample surface up to 100 C with respect to the ambient temperature. This effect vaporizes water and hence reduces the water content in the cement paste capillary pores hence reducing/removing any FT related ionic disjoining pressure. In addition, we found that adding a hydrophobic substance such carbon-black nanoparticles that dock into C-S-H large capillary pores readily improves the resistance to FT even in zero- electrical polarization conditions (see Figure 38). For the very same reason, the reduction/ annihilation of the ionic disjoining pressure in the wetting layer at the interface of the charged C-S-H pore surface and the surface of the growing phase, we think that the carbon-cement nanocomposites might also mitigate ASR.

Giving cement paste new properties and functionalities by doping it with carbon black or active carbon nanograins opens a new field of research and engineering. It is important to note that new compounds have to be economically viable, meaning that the additional phase to the cement paste has to be close to the cost of the cement itself. This is probably the case for black/activated carbons. LCA/LCCA studies have to be carried out to estimate the potential gain for implementing pavement solutions based on these new carbon-cement compounds under the invention that is covered by an MIT – CNRS patent filed in January 2019 [14].

5.4 Economic and environmental analyses of durable pavements

Quantification of the economic and environmental benefits of durable concrete pavements can be estimated when a tighter connection is established between the pavement damage models and long-term durability characterization. This remains a significant challenge and an opportunity for future research.

5.5 Towards understanding cement setting through molecular modeling and simulation

The molecular-level understanding of cement setting has been the scientific quest of the CSHub since its inception. It is the phenomenon that inspired the name "Liquid-Stone" that was adopted by the scientific research branch in the CSHub. Over the years there have been various contributions toward elucidating the three characteristic stages of strength evolution when cement powder is mixed with water. While we cannot yet claim cement paste hardening can be explained at the mechanism level and reproduced by molecular simulations, there now exists a body of research findings to suggest the mechanics aspects of the phenomenon are now coming under control. What still remain are the chemical aspects of cement hydration, such as the predicting and manipulating the effects of additives. This is an even more challenging task, but one which systematic studies through modeling and simulation along with well-designed measurements can begin to address.

Here we compile a selected list of our publications as evidence of gaining a deeper understanding cement setting, both to document the continuing work flow and for purposes of future reference.

- Self-consistent molecular model of C-S-H with a Ca/Si ratio of 1.7 and an appropriate C-S-H density of 2.3 gm/cc [15].
- Combinatorial optimization of computationally-generated database on cement paste with regard to calcium-silicon ratio, silicon-oxygen and calcium-oxygen distances [16]
- Mesoscale colloidal polydisperse model for nanomechanics studies of strength and hardness [17].
- Materials science perspective on concrete sustainability, nanomechanics of cement hardening [18].
- Commentary on cement setting as a materials challenge at the mesoscale science frontier [19].
- modeling water sorption and shrinkage in cement paste, pore blocking and drying and rewetting hystereses [20].
- Integrated mesoscale modeling of cement-paste texture, pore size distribution, and atomic configurations for interpretations of neutron small angle scattering, adsorption isotherms, and strength measurements on young cement paste [21].
- Molecular simulation of creep in a thin-film of metallic glass at laboratory time scales showing three stages of plastic deformation under an applied stress, demonstrating a close physical analogy to the three corresponding stages well known in cement setting [22].
- Molecular simulation of shear flow in a metallic glass model across three flow regimes spanning about 10 orders of magnitude in strain rate, further suggesting the physical basis for an analogy between rheologoical response of soft matter and the molecular mechanics of cement setting [23].

In summary, our recent work suggests the feasibility of probing the nanomechanical processes of gelation, incubation (C-S-H nucleation and growth), and hardening (percolation and jamming) in a single

simulation on the appropriate microstructure evolution time scale, thus providing a mesoscale explanation of the phenomenon that is the essence of cement science and technology.

References:

[1] Suraneni, P., et al., *A review of recent work on deicing salt damage to concrete pavements and its mitigation*

[2] Smith, S., et al., *Service-life of Concrete in Freeze-Thaw Environments: Critical Degree of Saturation and Calcium Oxychloride Formation. .* Cement and Concrete Research, Under review

[3] Collepardi, M., L. Coppola, and C. Pistolesi. *Durability of concrete structures exposed to $CaCl_2$ based deicing salts*. in *Proceedings of the 3rd CANMENT/ACI International Conference*. 1994. France: American Concrete Institute.

[4] Jones, W., et al., *An Overview of Joint Deterioration in Concrete Pavement: Mechanisms, Solution Properties, and Sealers*. 2013: West Lafayette, Indiana.

[5] Whatley, S.N., et al., *Mitigation of Calcium Oxychloride Formation in Cement Pastes Using Undensified Silica Fume.* Journal of Materials in Civil Engineering, 2017. **29**(10): p. 04017198.

[6] Suraneni, P., et al., *Calcium oxychloride formation in pastes containing supplementary cementitious materials: Thoughts on the role of cement and supplementary cementitious materials reactivity.* RILEM Technical Letters, 2016. **1**: p. 24-30.

[7] Suraneni, P., et al., *Use of fly ash to minimize deicing salt damage in concrete pavements.* Journal of the Transportation Research Board, 2017. **2629**: p. 24-32.

[8] Suraneni, P., et al., *Calcium oxychloride formation potential in cementitious pastes exposed to blends of deicing salt.* ACI Materials Journal, 2017. **114**(4): p. 631-641.

[9] Ghantous, R.M., et al., *Effect of accelerated carbonation conditions on the characterization of load-induced damage in reinforced concrete members.* Materials and Structures/Materiaux et Constructions, 2017. **50**(3).

[10] Todak, H., et al., *Freeze-Thaw resistance of concrete: The influence of air entrainment, water to cement ratio, and saturation* in *Proc. Int. Symp., Brittle Matrix Composites 11*. 2015. p. 101-109.

[11] Weiss, J., et al., *Toward Performance Specifications for Concrete Durability: Using the Formation Factor for Corrosion and Critical Saturation for Freeze-Thaw.* Transportation Research Board 2016.

[12] *Standard Method of Test for Characterization of the Air-Void System of Freshly Mixed Concrete by the* Sequential Pressure Method. AASHTO TP 118, 2015.

[13] J. Desarnaud, D. Bonn & N. Shahidzadeh, The Pressure induced by salt crystallization in confinement, Scientific Reports, **6**, 30856 | DOI: 10.1038/srep30856, 2016

[14] R. J.-M. Pellenq, A. Ioannidou, N. Chanut, R. Bakov, T. Divoux, F. Ulm, *Electron Conducting Carbon-Based Cement* - US PatentApp. 16/245,752, 2019.

[15] Pellenq, R.J.-M., et al., *A realistic molecular model of cement hydrates.* Proceedings of the National Academy of Sciences, 2009,**106**, 16102-16107.

[16] Abdolhosseini Oomi, M. J., et al., *Combinatorial Molecular Optimization of Cement Hydrates*. Nature Communications, 2016, **5**, 4960.

[17] Masoero, E., et al., *Nanostructure and Nanomechanics of Cement : Polydisperse, Colloidal Packing*. Physical Review Letters, 2012, **109**, 155503.

[18] Van Vliet, K., et al., *Set in sone? A perspective on the concrete sustainability challenge*. MRS Bulletin, 2012, **37**, 395-402.

[19] Yip, S. and Short, M.P., *Multiscale materials modelling at the mesoscale*. Nature Materials, 2013, **12**, 774-777.

[20] Pinson, M. B., et al., *Hysteresis from Multiscale Porosity: Modeling Water Sorption and Shrinkage in Cement Paste.* Physical Review Applied, 2015, **3**, 064009.

[21] Ioannidou, K., et al., *Mesoscale Texture of Cement Hydrates.* Proceedings of National Academy of Sciences, *2016,***113**, 2019-2034.
[22] Cao, P., et al., *Understanding the mechanisms of amorphous creep through molecular simulation.* Proceedings of National Academy of Sciences, 2017, **114**, 13631.
[23] Cao, P., et al., *Potential Energy Landscapes Governing plastic flows in glass rheology*. Proceedings of National Academy of Sciences, 2019, **116**, 18790.